Unruh-DeWitt detector response along static and circular-geodesic trajectories for Schwarzschild-AdS black holes

by

Keith K. Ng

A thesis
presented to the University of Waterloo
in fulfilment of the
thesis requirement for the degree of
Master of Science
in
Physics

Waterloo, Ontario, Canada, 2014

Author's declaration

I hereby declare that I am the sole author of this thesis. This is a true copy of the thesis, including any required final revisions, as accepted by my examiners.

I understand that my thesis may be made electronically available to the public.

Abstract

We present novel methods to numerically address the problem of characterizing the response of particle detectors in curved spacetimes. These methods allow for the integration of the Wightman function, at least in principle, in rather general backgrounds. In particular we will use this tool to further understand the nature of conformal massless scalar Hawking radiation from a Schwarzschild black hole in anti-de Sitter space. We do this by studying an Unruh-DeWitt detector at rest above the horizon and in circular geodesic orbit. The method allows us to see that the response rate shows peaks at certain characteristic frequencies, which correspond to the quasinormal modes (QNMs) of the spacetime. It is in principle possible to apply these techniques to more complicated and interesting physical scenarios, e.g. geodesic infall or multiple detector entanglement evolution, or the study of the behaviour of quantum correlations in spacetimes with black hole horizons.

Acknowledgements

I thank Eduardo Martín-Martínez for his advice during the project, and Robert B. Mann for being a wonderful supervisor.

This work was supported in part by the Natural Sciences and Engineering Research Council of Canada.

Contents

List of Figures

Chapter 1

Introduction

If science is about explaining physical phenomena, then the 20th century was a spectacular success for physics. The discovery of quantum mechanics, and the later development of the Standard Model, managed to provide a coherent description of the microscopic world, while general relativity explained the behaviour of the greater cosmos. In another respect, however, the many discoveries and successes suggested another problem. While both theories were, and are, highly accurate descriptions of their respective domains, they were completely incompatible. Quantum mechanics treats time as a special variable, while general relativity puts time and space on equal footing; gravity is non-renormalizable, and stubbornly refuses to be quantized (although neither issue has completely resisted progress; for more details see the discussion in Smolin [2005] and Bern et al. [2007]). Such incompatibilities have pushed the physicists of this century to come up with a new theory: one that explains both the very small and the very large, and everything in between.

One of the most important situations in which both theories come into play is the black hole. Being an object so massive that light cannot escape from it, general relativity naturally plays a large role in its description. However, Hawking [1974] used a quantum mechanical argument to conclude that black holes radiate as though they have a temperature. Since then, a great deal of research has been done to see how quantum mechanics and general relativity interact in this model system.

These investigations have lead to further questions, however. Current accepted theories predict that the Hawking radiation emitted by a black hole depends only on a small number of its physical properties; almost all information that falls in is lost. This is in direct contradiction with the

principle of unitarity in quantum physics, which states that information must be conserved. This information paradox is the most well-known problem concerning black hole physics, but other issues have also recently emerged (for instance, the question of black hole firewalls raised by Almheiri et al. [2013]). Understanding Hawking radiation is a first step towards resolving these issues.

One way of understanding a theory is to operationalize its definitions. Shortly after Hawking's paper, Unruh [1976] suggested the idea of a model particle detector in order to understand how an observer would go about "observing" the particles emitted by black holes, as well as the particles created by other phenomena (e.g. the Unruh effect). In more recent years, there has been much progress in verifying the existence of Hawking radiation in spacetimes with black hole event horizons using the Unruh-DeWitt detector formalism, a simplification of Unruh's original model. A recent proposal [Hodgkinson et al., 2014] has allowed for an insightful study of the thermal response of static and circular-geodesic particle detectors in Schwarzschild backgrounds, and there are new and promising results in progress regarding a detector model that is free from infrared divergences [Juárez-Aubry and Louko, 2014], which may be helpful in studying the response of particle detectors across event horizons.

In this thesis, we will analyze the radiation emitted by a black hole in a four-dimensional asymptotically anti-de Sitter space by means of the vacuum response of a particle detector in this background. This spacetime, often called "Schwarzschild-anti-de Sitter", or SAdS, has been examined by many other authors; however previous work has mostly focused on other aspects of the spacetime, such as characterizing the decay of scalar modes [Chan and Mann, 1997], analyzing its thermodynamics [Hawking and Page, 1983], calculating quasinormal frequencies [Horowitz and Hubeny, 2000, Daghigh and Green, 2009], and so on. While the Hawking radiation of the SAdS spacetime has previously been studied through other methods, e.g. [Hawking and Page, 1983, Hubeny et al., 2010], we believe that our application of particle detectors to the spacetime is novel, and shows new insights.

The selection of this spacetime is not without reason. AdS is not a description of the physical universe; it describes a universe with a negative cosmological constant, while astrophysical observations have revealed that our universe has a positive cosmological constant. However, some deep results in quantum mechanics have arisen from analysis of the AdS spacetime: for instance, Maldacena's celebrated discovery of AdS/CFT duality [Mal-

dacena, 1998] conjectured the equivalence of quantum gravitational physics inside AdS space with quantum field theory on its boundary. This thesis follows a large body of research into understanding AdS and related spacetimes, and using AdS and black holes to unify quantum physics and general relativity.

We begin with a brief review of the derivations of Hawking radiation. We then briefly review quantum field theory, before describing the Unruh-DeWitt detector, our model 'particle detector'. Next, we discuss the spacetime to be analyzed, the Schwarzschild-anti-de Sitter space. We describe our method of finding solutions to the Klein-Gordon equation in Schwarzschild-anti-de Sitter space, which will allow us to evaluate the Wightman function, and then use these solutions to calculate the response of the detector. We then explore some possible interpretations of the numerical results, and consider possible future avenues of research.

Chapter 2

Hawking radiation: a brief review

In 1974, Hawking published a letter [Hawking, 1974] positing that black holes should radiate particles as though they had a temperature. Specifically, he found that the temperature of a Schwarzschild black hole with surface gravity κ was $T_H = \kappa/2\pi$ (under geometrized units, i.e. $G = \hbar = c = k_B = 1$). The following year, Hawking published a paper [Hawking, 1975] with a somewhat more accessible derivation. While the derivation dealt with a spherical collapse spacetime in asymptotically flat space, following it is still quite useful; it illuminates certain issues that arise when considering more general spacetimes, and gives a general schema for calculating the production of particles on curved space.

For simplicity, consider a spherically symmetric spacetime which contains a collapsing null shell, with the conformal diagram seen in Fig. 2.1. Initially, the spacetime has no singularities; however, once the shell (i.e. the dashed line) collapses, a black hole forms in the centre, and an event horizon $\mathscr{H}$ appears. Generally speaking, if we wish to do quantum field theory on any spacetime, we must choose a basis of particles. Hawking's observation was that infinitely far away, it is fairly clear what we mean by a particle—after all, the spacetime is asymptotically flat, so we can just use the usual notions from flat space, relative to some stationary observer. However, to choose a basis, we must decide whether to consider the past infinity $\mathscr{I}^-$ or the future infinity $\mathscr{I}^+$. Each choice yields a different basis; by propagating modes on the future infinity backwards into the past, we can relate modes from the two bases. As it turns out, a positive frequency mode in the future corresponds

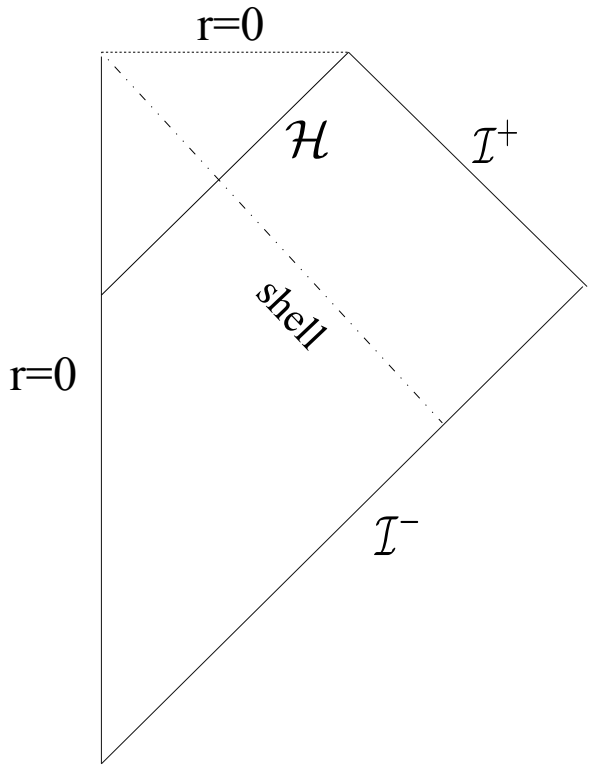

Figure 2.1: The conformal diagram of the collapse spacetime.

to a mixture of positive and negative frequency modes in the past. This mixing of positive and negative frequency modes means that the vacua of the two bases are not equivalent; a state with no particles in the past will have particles in the future. In other words, the collapse of the black hole produces particles.

However, there are a few subtleties involved in the derivation. One of the most important is that the derivation depends critically on a feature of the collapse spacetime known as global hyperbolicity: the notion that we can specify the state of the field at any point in space and time simply by specifying the state on an initial hypersurface, known as a Cauchy hypersurface. More specifically, Hawking used the fact that the solution on $\mathscr{I}^+$ can be determined from initial data from the past. Notably, the reverse is *not*

true: in order to determine the solution on $\mathscr{I}^-$, we would require not only data from $\mathscr{I}^+$, but also from the black hole singularity, or at least the black hole horizon $\mathscr{H}$.

Another subtlety is a consequence of the asymmetry mentioned above: because the black hole horizon exists only in the future, the basis of modes on the future infinity is not complete. In order to provide a complete basis, we would need to pick a set of modes on either the forming horizon or the singularity. However, since the spacetime is highly nonstationary, especially near the black hole, there is no natural way to define a particle basis there. (The difficulty of defining particles on time-dependent spacetimes is quite generic; for details one may refer to e.g. Birrell and Davies [1984].) Hawking's analysis sidestepped this difficulty by considering only the future modes that lived on the infinity; however, if we wish to do more quantum field theory on this spacetime, this uncertainty in the singularity basis becomes more problematic.

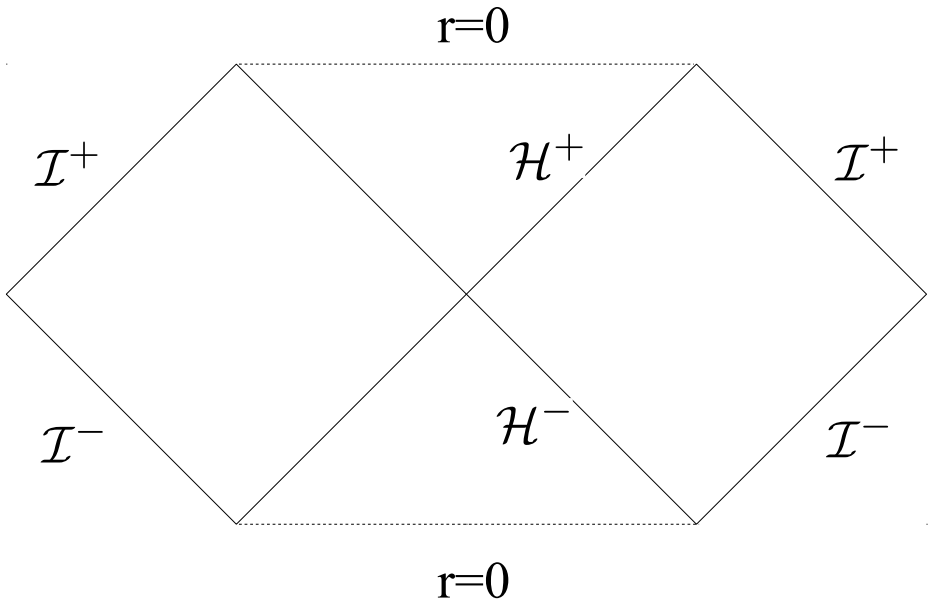

Figure 2.2: The conformal diagram of the extended Schwarzschild black hole.

The year after, Hawking collaborated with Hartle to produce another paper [Hartle and Hawking, 1976], this time dealing with the eternal Schwarzschild

black hole, which has the (extended) conformal diagram shown in Fig. 2.2. While the physicality of the spacetime was somewhat more tenuous—after all, such a black hole cannot, by definition, "form" from a collapse process—the spacetime possesses a few properties that facilitate analysis. One of the most important of these properties is that this spacetime is stationary. In particular, the dynamics of the field are time-independent, which makes calculations and interpretation very simple.

The derivation itself uses analytic continuation to link the state of the field on the external Schwarzschild spacetime to another manifold without singularities (the Euclidean Schwarzschild spacetime); the vacuum state of that other manifold is then "moved back" to the original spacetime. This method, known as Wick rotation, is a standard procedure in path-integral quantum field theory. As often occurs in Wick rotation, since the other manifold is periodic in (imaginary) time, the vacuum state on the Schwarzschild spacetime has a nonzero temperature; in other words, it has nonzero particle content. However, in terms of the modes defined on the extended manifold, known as Kruskal modes, the Hartle-Hawking state actually is a vacuum: there are no Kruskal particles in the Hartle-Hawking state. This can be used to facilitate calculations. As a bonus, the Hartle-Hawking state is smooth (i.e. without divergences) throughout the entire extended manifold.

However, the Hartle-Hawking state has a couple of peculiarities as well. To understand them, it is helpful to consider boundary conditions on the physical exterior only. Specifically, we consider the past and future infinity $\mathscr{I}^{\mp}$, as well as the past and future event horizons $\mathscr{H}^{\mp}$ of the black hole. (As we will later see, the wave equation near the horizon behaves almost exactly like the wave equation in flat space, so setting boundary conditions on the event horizon is not as unreasonable as it might seem.) The Hartle-Hawking state corresponds to a state that has no particles passing across either horizon $\mathscr{H}^{\pm}$. However, the particle flux across $\mathscr{I}^{\pm}$ is nonzero; in other words, not only does the Hartle-Hawking state feature particles escaping to infinity, but it also features particles falling in *from* infinity. Such a black hole would be in thermal equilibrium with its environment at all times, emitting and receiving equal amounts of radiation. This seems quite unphysical indeed!

This oddity of the Hartle-Hawking state led other researchers to consider other states, defined by other boundary conditions. Unruh [1976], for instance, considered the state in which particles are not present on either $\mathscr{I}^{-}$ or across $\mathscr{H}^{-}$; this choice is quite similar to the collapse scenario, where the asymptotic past is particle-free. Such a black hole behaves more as we

would expect a physical black hole to behave: it emits thermal radiation, but receives none in return. While this leads to divergences of the state on the past horizon $\mathscr{H}^-$, the more physical behaviour of this state lends it some attractiveness.

For completeness, we also consider the Boulware vacuum, which has no particles on $\mathscr{I}^\pm$. By definition, this state has no radiation; it is also divergent on both the horizons $\mathscr{H}^\pm$ of the black hole. However, it provides a useful point of comparison between vacua, in order to separate the effects of Hawking radiation from other effects that may exist.

Chapter 3

A brief introduction to quantum field theory in curved spacetime

A standard introduction to quantum theory often starts as follows: we consider a single particle, which possesses both position and momentum. We then 'promote' the position and momentum into *operators*, and enforce a canonical commutation relation. The result is a particle which cannot be completely localized; there is some uncertainty in its position and momentum which cannot be removed. We can also consider larger numbers of particles, add attractive or repulsive interactions between them, and so on. However, this picture does not suffice to explain the details of Hawking radiation. The most important deficiency is that in standard quantum mechanics, the number of particles always remains fixed. How can we model the *creation* of particles?

The solution to this problem is the recognition that the dynamics of the *field* are more fundamental than the dynamics of single particles. If we understand how the field evolves in time, not only can we understand how isolated particles behave, but we can also understand how particles can be created and destroyed. Therefore, we must find a way to quantize the field itself. While the usual presentation follows the historical development of the theory, going from particle 'solutions of the field equations' to field quantization on Minkowski space, and then generalizing to curved space, the review here will instead treat the field as fundamental from the beginning, and use the curved space generalization throughout. The reader may refer

to e.g. Fulling [1989] or Birrell and Davies [1984] for more information.

As in the particle case, we begin with the classical equations governing the field. For a spin-0 field, the relevant equation is the Klein-Gordon equation, which in Minkowski space is

$$\left[\left(\frac{d}{dt}\right)^2 - \nabla^2 + m^2\right]\phi = 0. \tag{3.1}$$

This is sometimes shortened further into

$$\left[-\Box + m^2\right]\psi = 0, \tag{3.2}$$

where $\Box = \eta^{\mu\nu}\partial_\mu\partial_\nu = \nabla^2 - (d/dt)^2$ is called the *d'Alembertian*, and $\eta_{\mu\nu} = \text{diag}[-1, +1, +1, +1]$ is the metric of Minkowski space. For simplicity, from now on we will set the mass $m = 0$. The quantization of the *massless* field is much like that of the massive field, but avoids some complications inherent in the latter.

Now, in the particle case, we would quantize both the particle's position and conjugate momentum. However, in the case of fields, it is not immediately obvious what the conjugate momentum of the field ϕ is. To determine the conjugate momentum, we pass to the Lagrangian (density) of the field theory. In Minkowski space, integrating the Lagrangian density $\mathcal{L}$ over all space and time results in the action

$$S = \int_{\mathbf{R}^N} d^N x \frac{1}{2}\left[-\eta^{\mu\nu}\partial_\mu\phi(x)\partial_\nu\phi(x) - m^2\phi(x)^2\right]. \tag{3.3}$$

The generalization of this action to curved space is fairly simple, with a couple of caveats. As we might expect, the partial derivatives must be replaced by covariant derivatives, and the Minkowski metric $\eta_{\mu\nu}$ by the curved metric $g(x)_{\mu\nu}$; however, some other changes are necessary. First, we add a term coupling the field to the scalar curvature R of the metric; the result is

$$L = \frac{1}{2}\left[-g(x)^{\mu\nu}\nabla_\mu\phi(x)\nabla_\nu\phi(x) - m^2\phi(x)^2 - \xi R(x)\phi(x)^2\right]. \tag{3.4}$$

This generalization of the Lagrangian is not completely arbitrary. Allowing $\xi \neq 0$ is quite useful; for instance, during renormalization procedures, the value of ξ often changes. More importantly, for $m = 0$, a special choice of ξ exists for which the Klein-Gordon equation becomes conformally invariant;

that is, if we conformally rescale the background spacetime, a valid solution to the equation is transformed into another valid solution. This value, for a spacetime with four dimensions, is $\xi = 1/6$ [Fulling, 1989].

Next, we must include a 'weight' to the Lagrangian, so that changes in the coordinate system do not affect the overall action. The correct weight in this case turns out to be $\sqrt{g}$, where $g = |det\,(g_{\mu\nu})|$ is the determinant of the metric; therefore, our new Lagrangian density is $\mathcal{L} = L\sqrt{g}$, and our new action is just the integral of $\mathcal{L}$ over the manifold $\mathcal{M}$,

$$S = \int_{\mathcal{M}} \mathcal{L}\, d^N x. \tag{3.5}$$

Given the Lagrangian density, we can then determine that the canonical momentum of the field is

$$\pi(x) = \frac{\partial \mathcal{L}}{\partial(\partial_0 \phi)} = -\sqrt{g}\, g^{0\nu} \partial_\nu \phi. \tag{3.6}$$

In the specific case of Minkowski space, of course, this is just the time derivative of the field ϕ. Finally, we impose the canonical (equal time) commutation relation on ϕ and π, namely

$$[\phi(t, \underline{x}), \pi(t, \underline{y})] = i\delta(\underline{x} - \underline{y}). \tag{3.7}$$

(We note here that a covariant commutation relation also exists. That relation treats time and space on an equal footing, but is somewhat less simple to define.)

We can also extract the curved-space generalization of the Klein-Gordon equation from the above Lagrangian. The corresponding Euler-Lagrange equation is

$$-\Box\phi + \left(m^2 + \xi R\right)\phi = 0, \tag{3.8}$$

where $\Box$ is the generalization of the d'Alembertian to curved space, namely

$$\begin{aligned} \Box\phi &= g^{\mu\nu} \nabla_\mu \nabla_\nu \phi \\ &= \frac{1}{\sqrt{g}} \partial_\mu \left[g^{\mu\nu} \sqrt{g}\, \partial_\nu \phi \right]. \end{aligned} \tag{3.9}$$

In the special case where the scalar curvature of the manifold is constant, the ξR term acts like an addition to the squared mass; note, however, that we

could also have ξR negative, which could result in an 'imaginary' effective mass.

There is one other issue to address: namely, what do states in the resulting Hilbert space 'look like'? While the details are rather subtle and technical, we could, for instance, attempt to construct an eigenstate of the field operator; more specifically, since $[\phi(t,\underline{x}),\phi(t,\underline{y})]=0$, we can construct a state which is an eigenstate of $\phi(t_0,\underline{x})$ for some particular $t=t_0$ Cauchy surface (or, more generally, over any Cauchy surface, although this is subtler). However, in many respects this is not ideal: since $\phi(t,\underline{x})$ and $\pi(t,\underline{y})$ do not commute, the field operator $\phi(t,\underline{x})$ clearly does not commute with the Hamiltonian

$$H=\int d^{N-1}x\,(\pi\,\partial_0\phi-\mathcal{L}), \tag{3.10}$$

so its evolution is not trivial, and in particular an eigenstate of $\phi(t_0,\underline{x})$ is generally not an eigenstate of $\phi(t,\underline{x})$ for $t\neq t_0$. (In fact, one can show that such a state has *infinite* energy, in the sense that a generalization of the uncertainty principle implies that such a state has totally uncertain momentum.)

While the representation of the Hilbert space in the general time-dependent case is rather tricky, one of the more popular approaches is as follows. We consider the full space of solutions to (3.8), and split it into positive and negative-frequency solutions; different choices of splitting lead to different physical theories. It is possible to then show that for any initial data ϕ on a Cauchy surface S, there exists a linear superposition of positive-frequency solutions which yield that initial data. Finally, picking a basis for the initial data yields 'normal modes', positive (negative) frequency solutions to (3.8) which correspond to the basis of initial data, and thus to annihilation (creation) operators, which we use to set up a Fock space. This is quite similar to the case of the harmonic oscillator, except instead of one mode, we have infinitely many; labelling the individual modes by j, for each positive (negative) frequency mode f_j (g_j), we associate annihilation and creation operators $a_j, a_j^\dagger$, and the commutation relation

$$\left[a_j, a_{j'}^\dagger\right]=\delta(j,j'). \tag{3.11}$$

(There are some subtleties involved in defining a delta function on a continuous space of labels; we will not discuss this further here.) Thus we have recovered some notion of 'particles' from our quantization of the field.

Finally, given the annihilation and creation operators of the Fock space, we can define a corresponding vacuum state $|0\rangle$, and repeatedly apply creation operators to populate the vacuum with particles. Since we used a complete basis of solutions to (3.8), we can therefore represent any state as a linear superposition of these particle eigenstates; one can show that the field operator can then be written

$$\phi(x) = \sum_j \left(a_j f_j(x) + a_j^\dagger g_j(x) \right), \tag{3.12}$$

where the 'summation' includes any necessary integrals. (To keep things simple, here we have absorbed various weighting factors into the normalization of f_j, g_j; in general one must be cautious about how they are normalized.)

While the above may seem like a rather unnecessarily complicated way to handle multiple particles, it is sufficiently general to apply to almost any (globally hyperbolic) space. For instance, in the case of the expanding FLRW universe, which is approximately Minkowski in the asymptotic past and future, one typically considers two different bases of particles: one which is positive-frequency (in the Minkowski sense) 'in the past', and one which is positive-frequency 'in the future'. In other words, one usually considers two different choices of positive-frequency solutions, one corresponding to each asymptotic limit. Notably, a mode which is positive frequency in the past is typically a mixture of positive and negative frequencies in the future, which one interprets as the creation of particles in the expanding FLRW universe (see e.g. Fulling [1989]).

The case of the Schwarzschild spacetime, shown in Fig. 2.2, is somewhat more complicated. Since it is static, we can simply choose the Cauchy surface $t = 0$, and we can pick a basis of modes which are eigenstates of the Hamiltonian, i.e. are of definite energy; this simplifies analysis greatly. However, there are multiple possible choices of positive-frequency modes; different choices of modes lead to different particle bases, and therefore different vacua. As mentioned earlier, the Klein-Gordon equation near the horizon approximates the equation on Minkowski space; so, both the horizons $\mathscr{H}^\pm$ and the infinities $\mathscr{I}^\pm$ of the spacetime are in some sense asymptotically Minkowski, and so we can identify modes with positive frequency on those surfaces as 'particles'. One can then define the *up* and *in* modes based on their asymptotic behaviours: near the past infinity $\mathscr{I}^-$, the *in* modes behave like incoming waves; near the past horizon $\mathscr{H}^-$, *up* modes behave like

outgoing waves. The Boulware vacuum, for instance, can then be described as the vacuum of *up* and *in* modes; it can be shown that a black hole in such a state does not radiate, and does not receive radiation.

However, one can define positive frequency on the Schwarzschild spacetime in another way. The Schwarzschild coordinates diverge at the horizon; for instance, an infalling observer will take an infinite amount of coordinate time t to reach the horizon $\mathscr{H}^+$. Therefore in order to allow for modes to "pass through" the horizon, we need a different parametrization of the extended manifold. One can do this using the Kruskal coordinates U, V, and then define positive frequency relative to those coordinates; the result is the basis of Kruskal modes, which correspond to the Hartle-Hawking vacuum. (This is the sense in which the Schwarzschild spacetime does not host particles 'going across the horizon', as mentioned in the previous chapter.) Of course, that means that the resulting modes do not 'look like' particles far from the black hole, so it is natural that the Hartle-Hawking vacuum contains particles relative to the Boulware vacuum; it radiates, and it receives radiation.

Lastly, the Unruh vacuum is a compromise between the two other vacua, being the vacuum of both the *in* modes and the outgoing Kruskal modes. This represents a black hole which radiates, but does not receive radiation. While this leads to singularities on the past horizon $\mathscr{H}^-$, this is ultimately not a major concern, since astrophysical black holes do not have a past horizon. In some sense, the Unruh vacuum is the best model for the black holes that live in our universe.

Ultimately, the general approach to getting particles from the quantized field has an ambiguity: there are many possible ways to choose 'positive-frequency' modes, each of which corresponds to a different definition of particle, and thus a different vacuum. In asymptotically-Minkowski and asymptotically-AdS spacetimes, clear choices exist, but in more general cases, there may be no natural way to select particles. In such a case, it may be prudent to abandon the notion of particles entirely.

Chapter 4

The Unruh-DeWitt detector

While the definition of particles on black hole spacetimes in terms of their behaviour on asymptotically flat limits is rigorous, it is rather unsatisfying. After all, we are used to talking about particles in a universe that is not flat everywhere, not even asymptotically. However, there are difficulties in defining particles in generic curved spacetimes; for instance, in the absence of a timelike Killing vector (i.e. on a time-dependent spacetime), there is no obvious choice of 'stationary' observers for which particles can be defined, and two different observers will often disagree about the particle content of any given state. (A simple example was illustrated by Fulling [1973].) So how can we understand the 'creation' of particles in more general situations?

One path forward was suggested by Unruh [1976]. In essence, Unruh considered a two-level system coupled to the local field; if the system becomes excited after interacting with the field, he argued, then we can conclude that excitations of the field (i.e. particles) exist. In other words, a particle is something that a particle detector detects. If we consider whether such a detector becomes excited in a generic spacetime, we can determine whether particles are created.

We model the particle detector with the Unruh-DeWitt model [DeWitt, 1980], a simplification of Unruh's original concept. It consists of a two-level system with a monopole coupling to a scalar field. Although simple, this model is known to capture the fundamental features of the light-matter interaction [Scully and Zubairy, 1997] when no orbital angular momentum exchange between atomic electrons and the electromagnetic (EM) field is involved [Martín-Martínez et al., 2013, Alhambra et al., 2014]. The coupling

is given by the interaction Hamiltonian

$$H_{\text{int}}(\tau) = c\chi(\tau)\mu(\tau)\phi(x(\tau)), \tag{4.1}$$

where c is a coupling constant, $\chi(\tau)$ is the switching function, μ is the detector's monopole moment operator, $x(\tau)$ is the trajectory of the detector, and τ is the proper time of the detector (henceforth simply 'proper time'). If the initial state of the joint system is $|\Psi\rangle \otimes |0\rangle_d$ where $|\Psi\rangle$ is a Hadamard state, on which the expectation of the energy-momentum tensor is non-singular, and if c is small, one can write the transition probability (summing over all final field configurations) to first order in perturbation theory as [Louko and Satz, 2008]

$$P(E) = c^2 \left|{}_d \langle 0 \left| \mu(0) \right| 1 \rangle_d \right|^2 F(E), \tag{4.2}$$

where the response function $F(E)$ is independent of the physical details of the detector, aside from its dependence on the detector's energy gap E. For instance, this form holds whether the detector is a two-level system or a harmonic oscillator; the differences only become apparent at higher order in perturbation theory and do not yield a qualitative difference as compared with the two-level quantum emitter [Brown et al., 2013]. For this reason, abusing notation, the response function itself is often simply called the 'probability' [Louko and Satz, 2008]. The response function can be written as

$$\begin{aligned} F(E) = \lim_{\epsilon \to 0} \int_{-\infty}^{\infty} \mathrm{d}u \, \chi(u) \\ \times \int_{-\infty}^{\infty} \mathrm{d}s \, \chi(u-s) e^{-iEs} W_\epsilon(u, u-s) \end{aligned} \tag{4.3}$$

where $W(u, u') = W(x(u), x(u'))$ is the pullback of the Wightman function $W(x, x') = \langle \Psi \left| \phi(x)\phi(x') \right| \Psi \rangle$ to the detector trajectory and ϵ parametrizes its regularization.

As a side note, while the Wightman function itself is less frequently used than some of the other Green's functions, in the particular case where $t > t'$, the Wightman function $W(x, x')$ is equal to the more familiar Feynman propagator $G_F(x, x') = \langle \Psi \left| T(\phi(x)\phi(x')) \right| \Psi \rangle$. Both functions describe the correlations in the field; most methods of calculating one can be adapted to calculate the other.

In the special cases where the detector is static, or on a circular geodesic orbit, and its response integrated over all times, no special considerations are

required to regularize the Wightman function or to control possible divergences related to the switching function; in this case, the Wightman function only depends on the proper time between points, $W(u, u-s) = W(s)$, as discussed in Hodgkinson [2013]. The response function can then be written as

$$F(E) = \lim_{\epsilon \to 0} \int_{-\infty}^{\infty} \mathrm{d}u \int_{-\infty}^{\infty} \mathrm{d}s \, e^{-iEs} W_\epsilon(s), \tag{4.4}$$

and taking the time derivative (i.e. dropping the u integral) yields the transition rate

$$\dot{F}(E) = \lim_{\epsilon \to 0} \int_{-\infty}^{\infty} \mathrm{d}s \, e^{-iEs} W_\epsilon(s). \tag{4.5}$$

More precisely, we have taken the limit in which the detector is on for an infinite time; this removes any transient effects due to switching which may induce additional detector excitation [Louko and Satz, 2008]. However, there may still be other features inherent in the response function which contain information about the particular spacetime background, as will be demonstrated.

Readers familiar with the background of Unruh-DeWitt detectors may notice a certain omission in the description above. It was previously stated that excitation of the detector implies detection of a particle. However, it is well-known (see e.g. Unruh [1976]) that accelerated detectors can become excited even when no particles exist, e.g. the Minkowski vacuum; this phenomenon is known as the Unruh effect. For this reason, we might expect a detector in circular geodesic orbit, for instance, to become excited independent of the existence of Hawking radiation. Fortunately, there is a point of comparison: by comparing the Boulware vacuum, which has no Hawking radiation, to other vacua, we can determine what contribution is due to Hawking radiation, and what contribution is due merely to other effects.

Chapter 5

The SAdS metric

While our previous discussion has focused on the generalities of detecting Hawking radiation, we must choose a particular spacetime to proceed further. The Schwarszchild spacetime is in many ways the simplest and most physically relevant; however, it has also previously been analyzed by Hodgkinson [2013]. Therefore, we consider a more general spacetime, namely Schwarzschild-anti-de Sitter, in which the cosmological constant is negative, rather than zero. While this scenario is less physically relevant (in our universe, the cosmological constant is extremely small, but positive), it is still of some importance: for instance, the AdS/CFT duality concerns this sort of spacetime. Therefore, this spacetime merits further study.

The spacetime known as "Schwarzschild-anti-de Sitter", Schwarzschild-AdS, or simply SAdS, has the following metric [Hawking and Page, 1983]:

$$ds^2 = -f(r)dt^2 + f(r)^{-1}dr^2 + r^2 d\Omega_2^2, \tag{5.1}$$

where the lapse function $f(r)$ is given by

$$f(r) = \frac{r^2}{L^2} + 1 - \frac{r_0}{r}, \tag{5.2}$$

$L = \sqrt{-3/\Lambda}$ is the AdS characteristic length, and $r_0 = 2M$. Since, without losing generality, one is free to choose an arbitrary value for one of the length scales (equivalent to assuming some system of units), for convenience we set $L = 1$. Its conformal diagram is shown in Fig. 5.1.

This spacetime has a few notable features. Like AdS, its 'conformal infinity' I is timelike; that is, signals can propagate from spatial infinity to any

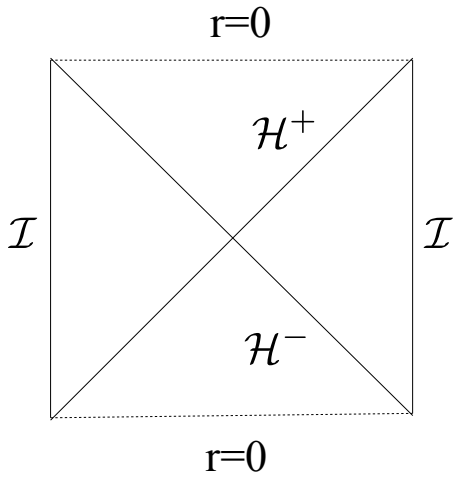

Figure 5.1: The conformal diagram of the extended Schwarzschild-AdS black hole.

point in Schwarzschild-AdS in finite coordinate time (i.e. finite t). As we will discuss later, this introduces some unique problems. As the SAdS spacetime is asymptotically AdS, we can also inherit the notion of 'particles' from AdS, much as Schwarzschild spacetimes inherit their definition of particles from Minkowski space. Like Schwarzschild, it has an event horizon r_+ — namely, the largest (real) root of the lapse function $f(r)$. The domain of interest is $r_+ < r < \infty$. Note that one can write $r_0 = r_+(r_+^2 + 1)$; since this expression cannot be easily inverted, r_+ is the more convenient parametrization of the black hole size.

For later use, we also define the tortoise coordinate, defined by $dr^* = dr/f(r)$; this new parametrization reaches a finite value as $r \to \infty$, and $r^* \to -\infty$ as $r \to r_+$. Since r^* is defined up to a constant, we choose to set $r^* = 0$ at infinity; in other words,

$$r^* = -\int_r^\infty \frac{dr'}{f(r')}. \tag{5.3}$$

We also define the null coordinates, $u = t - r^*$ and $v = t + r^*$, and the

Kruskal coordinates

$$U = -\exp(-2\pi T_H u) \tag{5.4}$$

$$V = \exp(2\pi T_H v) \tag{5.5}$$

where

$$\begin{aligned} T_H &= \frac{1}{4\pi} f'(r_+) \\ &= \frac{3r_+^2 + 1}{4\pi r_+} \end{aligned} \tag{5.6}$$

is the usual Hawking temperature. (This can be derived in a similar way as in the Schwarzschild case, by considering Wick rotation, and removing the singularity that appears by periodic identification of imaginary time; refer to Hawking and Page [1983] for details.) As in the Schwarzschild case, the Kruskal coordinates can be used to remove the divergence of the metric at the event horizon.

Chapter 6

Quantum field theory on SAdS

6.1 The Klein-Gordon equation

Recall the Klein-Gordon equation derived earlier for curved space (3.8):

$$-\Box\phi + \left(m^2 + \xi R\right)\phi = 0, \tag{6.1}$$

Most papers analyzing SAdS space have focused on minimally coupled fields, $\xi = 0$; see Berti et al. [2009] for a recent review. This type of coupling generalizes quite readily to massive fields and fields of nonzero spin, e.g. gravitational waves. However, in this thesis, we will instead focus on the conformally coupled massless scalar field, $\xi = 1/6$. The conformal coupling was chosen because it most closely mimics the more astrophysically relevant case of the Schwarzschild black hole in flat space—namely, that the effective potential takes a finite value at infinity (if not necessarily zero), and that the effective potential always has a maximum outside the horizon. Note that this potential was previously explored by Chan and Mann [1997].

Since the conformal infinity $\mathscr{I}$ of an asymptotically anti-de Sitter space is timelike, one must also specify a boundary condition at infinity. This choice is quite important: the quantization of the scalar field differs drastically depending on what boundary condition we choose. The usual possibilities are often known as 'reflecting' and 'transparent'. While we could, in principle, choose to make the boundary transparent, i.e. allow particles to escape, the corresponding quantization has some very undesirable properties—for instance, the space is no longer globally hyperbolic, unless embedded in some larger space, e.g. the Einstein static universe. However, this procedure causes

other peculiarities: for instance, particles exiting one side of the universe re-enter through the opposite side after some finite coordinate time. The reader may refer to Avis et al. [1978] for more information. (In principle, we could also define a quantum field theory, with attendant modes, *on* the conformal boundary; in fact, this is exactly the case in which an AdS/CFT duality may appear. However, this is rather sophisticated, and we will not discuss it further; see Witten [1998] for a brief overview.)

Instead, we will take the usual Dirichlet (i.e. reflective) boundary conditions—that is, where mode functions vanish at infinity, and particles cannot escape. The quantization corresponding to this choice does not suffer the non-local behaviours inherent with the transparent case [Avis et al., 1978]. However, it is easier to start by analyzing the usual incoming and outgoing modes as if the conformal infinity actually were transparent, and then find a linear superposition satisfying the physical boundary conditions.

Because of the high degree of symmetry inherent in the SAdS spacetime, the Klein-Gordon equations are separable; the solutions to the angular part are the usual spherical harmonics, for instance. If one writes the solutions to the Klein-Gordon equation as [Horowitz and Hubeny, 2000]

$$\begin{aligned} w^{in}_{\omega lm} &= (4\pi\omega)^{-1/2} r^{-1} \psi^{in}_{\omega l}(r) Y_{lm}(\theta,\phi) e^{-i\omega(t+r^*)} \\ w^{out}_{\omega lm} &= (4\pi\omega)^{-1/2} r^{-1} \psi^{out}_{\omega l}(r) Y_{lm}(\theta,\phi) e^{-i\omega(t-r^*)}, \end{aligned} \tag{6.2}$$

where m refers to angular momentum and *not* mass, the radial equations become

$$\begin{aligned} f(r)\frac{d^2}{dr^2}\psi^{in}_{\omega l}(r) + [f'(r) - 2i\omega]\frac{d}{dr}\psi^{in}_{\omega l}(r) \\ -V(r)\psi^{in}_{\omega l}(r) = 0, \end{aligned} \tag{6.3}$$

$$\begin{aligned} f(r)\frac{d^2}{dr^2}\psi^{out}_{\omega l}(r) + [f'(r) + 2i\omega]\frac{d}{dr}\psi^{out}_{\omega l}(r) \\ -V(r)\psi^{out}_{\omega l}(r) = 0, \end{aligned} \tag{6.4}$$

where

$$V(r) = \frac{l(l+1)}{r^2} + \frac{r_0}{r^3} \tag{6.5}$$

for a conformal coupling. Note that $\psi(r)$ approaches a finite value near the horizon; for simplicity we will set $\psi(r_+) = 1$.

As a side note, if we use the tortoise coordinates r^* instead, the one-dimensional Klein-Gordon equation takes a very simple form:

$$[\partial_{r^*}^2 + \omega^2 - \tilde{V}(r^*)](rw_{\omega lm}) = 0, \tag{6.6}$$

where the effective potential

$$\tilde{V}(r^*) = f(r^*)V(r^*) = f(r)\left(\frac{l(l+1)}{r^2} + \frac{r_0}{r^3}\right)$$

vanishes near the horizon. In the particular case considered here, that of the massless conformal scalar, the effective potential has a finite value near infinity as well; specifically, $\tilde{V}(r \to \infty) = l(l+1)$. This implies that much like the case of the Schwarzschild black hole in flat space, there are modes defined for $r < \infty$ where $\Phi \sim r^{-1}e^{-i\omega(t\pm r^*)}$; this is why we have named the solutions to (6.2) 'in' and 'out'. However, while this form illuminates some of the key behaviours of the field on this spacetime, it is not quite as useful for purposes of calculation, since r and r^* are related by an integral; in particular, calculating the effective potential $\tilde{V}(r)$ in terms of r^* is quite computationally expensive. As well, since the oscillatory term has not been separated from the rest of the mode, solutions to this equation will diverge near the horizon. We therefore focus on solving the previous equations (6.2).

Let us make a note here regarding the effective potential, $\tilde{V}(r) = f(r)V(r)$. In contrast to the minimally coupled case, here the effective potential goes to a finite value as $r \to \infty$. Furthermore, this effective potential always has a maximum above the event horizon for any r_+; this is in contrast to the minimally coupled case, where the effective potential for a sufficiently large black hole will not have a local maximum above the event horizon [Berti et al., 2009]. Therefore, one does not expect to see phenomena related to the phase transition.

As stated earlier, precisely because we want spatial infinity to be reflecting, these 'in' and 'out' modes are not typically valid solutions. They do behave correctly everywhere *except* spatial infinity; if one were to apply a conformal transformation to the interval of interest to make it finite, the in and out modes would simply take the wrong value at the point corresponding to spatial infinity. Nevertheless, one can find a linear superposition of them which satisfies the boundary condition. Notice that for real ω, the equations governing the in and out modes are complex conjugates; so, in that case $\psi_{\omega l}^{out} = \psi_{\omega l}^{in*}$.

We now characterize the physical modes $w_{\omega lm}$ in terms of the in and out modes defined in (6.2). For ω positive, the ψ parts of the in and out modes are complex conjugates. Hence, if we can determine $\theta_0 = \mathrm{ph}[\psi^{in}_{\omega l}(r \to \infty)]$, then we know that a solution to the Klein-Gordon equation satisfying the boundary conditions is

$$\begin{aligned} w_{\omega lm} &= (4\pi\omega)^{-1/2} r^{-1} e^{-i\omega t} Y_{lm}(\theta, \phi) \\ &\quad \times (-i) \left(e^{-i\theta_0} e^{-i\omega r^*} \psi^{in}_{\omega l} - e^{i\theta_0} e^{i\omega r^*} \psi^{out}_{\omega l} \right) \end{aligned} \tag{6.7}$$

or simply

$$\begin{aligned} w_{\omega lm} &= (4\pi\omega)^{-1/2} r^{-1} e^{-i\omega t} Y_{lm}(\theta, \phi) \\ &\quad \times 2\,\mathrm{Im}\left(e^{-i(\theta_0 + \omega r^*)} \psi^{in}_{\omega l} \right). \end{aligned} \tag{6.8}$$

For brevity, let us define the time-independent radial part of the mode as

$$R_{\omega l}(r) = r^{-1} 2\,\mathrm{Im}\left(e^{-i(\theta_0 + \omega r^*)} \psi^{in}_{\omega l} \right). \tag{6.9}$$

$R_{\omega l}$ is independent of m; this is a consequence of the spherical symmetry of SAdS. In particular, if the black hole were rotating, the radial part of the modes would depend on m. The reason we included the 2 is so that $\tilde{R}_{\omega l} = r R_{\omega l}$ satisfies the Schrödinger normalization,

$$\int_{-\infty}^{0} \mathrm{d}r^* \tilde{R}_{\omega l} \tilde{R}^*_{\omega' l} = 2\pi\delta(\omega - \omega'). \tag{6.10}$$

Note that (6.9) immediately implies that the time-independent radial part of the mode is real.

A cursory examination of the equations governing the metric and the modes suggests that rescaling to a different value of L is fairly simple, with a couple caveats. Time and space coordinates scale in the obvious way: $t \to \sigma t$, $r \to \sigma r$. As one might expect, temperature, energy, and transition rate scale inversely with σ, i.e. $T_H \to T_H/\sigma$, $\omega \to \omega/\sigma$, and $\dot{F}(E) \to \dot{F}(E/\sigma)/\sigma$. Therefore, E/T_H is invariant under scaling, as is the product of $\dot{F}$ and any of the three lengths r_+, r_0, and L. Notably, $f(r) \to f(\sigma r)$; the lapse function at equivalent radii is scale-invariant. In this thesis, we will use ωL and $L\dot{F}$ to refer to the dimensionless energy and transition rate respectively.

6.2 The Hartle-Hawking vacuum

We first consider the Hartle-Hawking vacuum, which corresponds to a black hole which emits Hawking radiation in equilibrium with its environment. As usual, one can write the field operator as

$$\phi(x) = \sum_{l=0}^{\infty} \sum_{m=0}^{\infty} \int_0^{\infty} d\omega \left(a_{\omega lm} w_{\omega lm} + a^{\dagger}_{\omega lm} w^*_{\omega lm} \right), \tag{6.11}$$

where $a_{\omega lm}$ is the annihilator of the physical mode of energy ω and angular momentum quantum numbers l, m and $w_{\omega lm}$ is the corresponding solution to the Klein-Gordon equation. (Compare (3.12).)

In order to calculate the response function, we then need to calculate how the Wightman function of the Hartle-Hawking vacuum depends on the modes. Recall that the Hartle-Hawking vacuum is the vacuum corresponding to the Kruskal modes (i.e. modes which cover both the inside and outside of the black hole); therefore, to calculate the Wightman function, we can relate the external modes and the Kruskal modes via Bogoliubov transformations. The derivation works in a similar way as in the asymptotically flat Schwarzschild case; the details can be found in Appendix A. The result is that

$$\begin{aligned} W(x, x') = \sum_{l=0}^{\infty} \sum_{m=-l}^{l} \int_0^{\infty} \frac{d\omega}{2 \sinh(\omega / 2T_H)} \\ \left[e^{\omega / 2T_H} w_{\omega lm}(x) w^*_{\omega lm}(x') \right. \\ \left. + e^{-\omega / 2T_H} w^*_{\omega lm}(x) w_{\omega lm}(x') \right]. \end{aligned} \tag{6.12}$$

We can then write the Wightman function in terms of the radial modes defined in (6.9):

$$\begin{aligned} W(x, x') = \sum_{l=0}^{\infty} \sum_{m=-l}^{l} \int_0^{\infty} \frac{d\omega}{8\pi\omega \sinh(\omega / 2T_H)} \\ \times \left[e^{\omega / 2T_H - i\omega(t-t')} Y_{lm}(\theta, \phi) Y^*_{lm}(\theta', \phi') R_{\omega l}(r) R_{\omega l}(r') \right. \\ \left. + e^{-\omega / 2T_H + i\omega(t-t')} Y^*_{lm}(\theta, \phi) Y_{lm}(\theta', \phi') R_{\omega l}(r) R_{\omega l}(r') \right]. \end{aligned} \tag{6.13}$$

This expression is almost identical to that of the Schwarzschild case (see Hodgkinson [2013])—in fact, it *is* identical, after substituting the appropriate

T_H and $R_{\omega l}(r)$ functions. Of course, the key difference is that one only has one set of basis functions. Note that this expression for the Wightman function allows us to use essentially the same expression for the transition rate of the static detector as in the Schwarzschild case, with the substitutions noted above.

In the specific case of the static detector, we can simplify even further. The proper time between t and t' is then just $s = \sqrt{f(r)}(t - t')$, i.e. $(t - t') = s/\sqrt{f(r)}$. By spherical symmetry, it suffices to consider the case where $\theta = \theta' = 0$. In that case,

$$Y_{lm}(\theta = 0, \phi) = \delta_{m,0}\sqrt{\frac{2l+1}{4\pi}},$$

and thus (the pullback to the worldline of) the Wightman function, $W(s) = W(u, u - s)$, may be written

$$\begin{aligned}
W(s) =& \sum_{l=0}^{\infty} \int_0^{\infty} \frac{(2l+1)\, d\omega}{32\pi^2 \omega \sinh(\omega/2T_H)} \\
& \times \Big[e^{\omega/2T_H - i\omega s/\sqrt{f(r)}} \\
& + e^{-\omega/2T_H + i\omega s/\sqrt{f(r)}} \Big] R^2_{\omega l}(r) \\
=& \sum_{l=0}^{\infty} \int_0^{\infty} \frac{(2l+1)\, d\omega}{16\pi^2 \omega \sinh(\omega/2T_H)} \\
& \times \cos\left[\omega \left(\frac{s}{\sqrt{f(r)}} + \frac{i}{2T_H} \right) \right] R^2_{\omega l}(r) \\
=& \sum_{l=0}^{\infty} \int_0^{\infty} d\omega\, \frac{(2l+1)}{16\pi^2 \omega} R^2_{\omega l}(r) \\
& \times \Big[\coth(\omega/2T_H) \cos(\omega s/\sqrt{f(r)}) \\
& - i \sin(\omega s/\sqrt{f(r)}) \Big]
\end{aligned} \tag{6.14}$$

where r is the radius at which the static detector is located. We can then simply substitute this into (4.5) to calculate the transition rate; following the derivation in Hodgkinson [2013], this yields

$$\dot{F}(E) = \frac{1}{2E} \frac{1}{e^{E/T_{loc}} - 1} \sum_{l=0}^{\infty} \frac{2l+1}{4\pi} R^2_{\tilde{\omega} l}(r), \tag{6.15}$$

where $\tilde{\omega} = \sqrt{f(r)}E$ and $T_{loc} = T_H/\sqrt{f(r)}$. Notice that since the remaining integral in (4.5) evaluates to a Dirac delta, one only needs to evaluate the mode at one value of ω for each l.

We can also consider the case where the detector is in a circular geodesic orbit at radius r. For convenience, we will write:

$$\begin{aligned} a &:= dt/d\tau = \sqrt{\frac{2r}{2r-3r_0}} \\ b &:= d\phi/d\tau = \sqrt{\frac{r_0+2r^3}{r^2(2r-3r_0)}} \end{aligned} \tag{6.16}$$

The transition rate of a detector in a circular geodesic orbit can then be found to be [Hodgkinson, 2013]

$$\begin{aligned} \dot{F}(E) =& \sum_{l=0}^{\infty}\sum_{m=-l}^{l} \frac{(l-m)!}{(l+m)!}\frac{2l+1}{16\pi}|P_l^m(0)|^2 \\ &\times \left(\Theta(\omega_-)\frac{e^{2\pi\omega_-}}{a\omega_-\sinh(2\pi\omega_-)}R^2_{\omega_- l}(r)\right. \\ &\left. + \Theta(\omega_+)\frac{e^{-2\pi\omega_+}}{a\omega_+\sinh(2\pi\omega_+)}R^2_{\omega_+ l}(r)\right) \end{aligned} \tag{6.17}$$

where $\omega_\pm = \frac{mb\pm E}{a}$ is a function of m, and $P_l^m(x)$ is the associated Legendre polynomial. Notice that, since one must sum over a number of m proportional to l for each l, the total number of modes evaluated is of order l^2. This is in contrast to the static case, where one only needed to calculate one mode for every l, namely at $m = 0$. (While one can take advantage of certain symmetries of $P_l^m(0)$ to shorten the calculation, the general scaling relation still holds.)

At this point, it should be noted that $V_l(r)$ near the horizon, $r \approx r_+$, behaves like

$$V_l(r) \approx \frac{1}{r^2}\left(l(l+1) + (r_+^2+1)\right). \tag{6.18}$$

This is rather problematic: It means that for large r_+—the case which is most interesting from the AdS/CFT perspective—one will need to calculate the Wightman function and modes to high angular momentum, of order r_+. In particular, since the circular geodesic calculation requires $O(l^2)$ mode calculations, that calculation can quickly become intractable. However, this is unavoidable given the mode separation method. On the other hand, for small r_+, one will only need to worry about very small angular momenta.

6.3 The Boulware vacuum

We will also consider the vacuum in which static observers outside the horizon observe no particles; this is known as the Boulware vacuum. In other words, this is the vacuum corresponding to the usual external modes. The Wightman function of the Boulware vacuum is

$$\begin{aligned} W(x,x') &= \langle\Psi|\,\phi(x)\phi(x')\,|\Psi\rangle \\ &= \sum_{l=0}^{\infty}\sum_{m=-l}^{l}\int_0^\infty \frac{d\omega}{4\pi\omega} \\ &\times \left[e^{-i\omega(t-t')}Y_{lm}(\theta,\phi)Y^*_{lm}(\theta',\phi')R_{\omega l}(r)R_{\omega l}(r')\right], \end{aligned} \tag{6.19}$$

while the static detector response rate is simply

$$\dot{F}(E) = \Theta(-E)\frac{1}{2|E|}\sum_{l=0}^{\infty}\frac{2l+1}{4\pi}R^2_{\tilde{\omega}l}(r), \tag{6.20}$$

and the circular detector response is (using the quantities defined in (6.16))

$$\begin{aligned} \dot{F}(E) =& \frac{1}{a}\sum_{l=0}^{\infty}\sum_{m=-l}^{l}\frac{(l-m)!}{(l+m)!}\frac{2l+1}{8\pi\omega_-}|P^m_l(0)|^2 \\ &\times \Theta(\omega_-)R^2_{\omega_- l}(r) \end{aligned} \tag{6.21}$$

where $\omega_- = \frac{mb-E}{a}$ as before.

Comparing the Boulware and Hartle-Hawking vacua allows us to determine the effect of Hawking radiation, separate from any other possible effects on the response of the detector.

6.4 The Unruh vacuum does not exist

At this point, one might also consider the Unruh vacuum, in which the black hole emits particle radiation, but does not receive particle radiation from its environment. However, because we chose to make the conformal infinity reflective, this is not possible; any radiation emitted by the black hole will be reflected off infinity and return to it. Since we prefer to consider stationary vacuum states, this means that no 'Unruh-like' vacuum can exist. Therefore, the only two vacua that may be considered are the Boulware and Hartle-Hawking vacua.

6.5 Solving the Klein-Gordon equation numerically

The method used to solve the Klein-Gordon equation is similar to a previous method first used by Horowitz and Hubeny [2000] to find the quasinormal modes of a minimally coupled scalar in Schwarzschild-AdS; we use it to find modes of the conformally coupled scalar.

We apply a transformation to the radial part of the solutions to the Klein-Gordon equation, substituting $x = 1/r$. Letting $x_+ = 1/r_+$, we find that the in and out radial solutions satisfy

$$s(x)\frac{d^2}{dx^2}\psi^{in}_{\omega l}(x) + \frac{t^{in}(x)}{x - x_+}\frac{d}{dx}\psi^{in}_{\omega l}(x) + \frac{u(x)}{(x - x_+)^2}\psi^{in}_{\omega l}(x) = 0 \tag{6.22}$$

$$s(x)\frac{d^2}{dx^2}\psi^{out}_{\omega l}(x) + \frac{t^{out}(x)}{x - x_+}\frac{d}{dx}\psi^{out}_{\omega l}(x) + \frac{u(x)}{(x - x_+)^2}\psi^{out}_{\omega l}(x) = 0 \tag{6.23}$$

where

$$s(x) = \frac{x_+^2 + 1}{x_+^3}x^4 + \frac{1}{x_+^2}x^3 + \frac{1}{x_+}x^2 \tag{6.24}$$

$$t^{in}(x) = 3r_0x^4 - 2x^3 - 2x^2 i\omega \tag{6.25}$$

$$t^{out}(x) = 3r_0x^4 - 2x^3 + 2x^2 i\omega \tag{6.26}$$

$$u(x) = (x - x_+)V(x). \tag{6.27}$$

We then expand the solutions around the horizon x_+:

$$\psi^{in}_{\omega l}(x) = \sum_{n=0}^{\infty} a^{in}_n (x - x_+)^n \tag{6.28}$$

$$\psi^{out}_{\omega l}(x) = \sum_{n=0}^{\infty} a^{out}_n (x - x_+)^n; \tag{6.29}$$

the coefficients then are governed by the recurrence relations

$$a_n^{in} = -\frac{1}{P_n^{in}} \sum_{k=0}^{n-1} [k(k-1)s_{n-k} + kt_{n-k}^{in} + u_{n-k}]a_k^{in} \tag{6.30}$$

$$a_n^{out} = -\frac{1}{P_n^{out}} \sum_{k=0}^{n-1} [k(k-1)s_{n-k} + kt_{n-k}^{out} + u_{n-k}]a_k^{out} \tag{6.31}$$

where

$$s(x) = \sum_{n=0}^{4} s_n (x - x_+)^n \tag{6.32}$$

$$t^{in}(x) = \sum_{n=0}^{4} t_n^{in} (x - x_+)^n \tag{6.33}$$

$$t^{out}(x) = \sum_{n=0}^{4} t_n^{out} (x - x_+)^n \tag{6.34}$$

$$u(x) = \sum_{n=0}^{4} u_n (x - x_+)^n \tag{6.35}$$

$$P_n^{in} = n(n-1)s_0 + nt_0^{in} \tag{6.36}$$

$$P_n^{out} = n(n-1)s_0 + nt_0^{out}. \tag{6.37}$$

Note that the recurrence relations (6.30), (6.31) only involve a finite number of a_k terms (five, in this case), as $s(x)$, $t(x)$ and $u(x)$ are all quartic polynomials.

As mentioned earlier, these solutions do not satisfy the boundary condition at infinity. Specifically, because of the structure of (6.22), the expressions in (6.28), (6.29) will diverge at $x = 0$. However, summing over a finite number of terms N at $x = 0$ allows us to find a linear combination of those modes which vanishes at $x = 0$; in other words, one can solve for A, B such that

$$A \sum_{n=0}^{N} [a_n^{in}(-x_+)^n] + B \sum_{n=0}^{N} [a_n^{out}(-x_+)^n] = 0. \tag{6.38}$$

One can then increase N and verify that the linear combination still vanishes. In the particular case where ω is real, the in and out modes are complex

conjugates, so this must be possible; we use the approach described in the previous section, culminating in (6.9).

For smaller values of ω, smaller l, and near the horizon, the power series expression for $\psi^{in}_{\omega l}$ can be found with a reasonable value of N. However, for larger values of ω, larger l and for larger radii, convergence takes a very large number of terms; in particular, it is more efficient to compute the values of the modes at spatial infinity using another approach, e.g. using the power series expansion at finite distance and numerically integrating the differential equation to spatial infinity.

Note that this method is somewhat different from the approach taken by Horowitz and Hubeny [2000]. Since they were interested in quasinormal modes, they only considered modes that were ingoing at infinity; they then solved for complex ω such that $\sum_{n=0}^{N}[a^{in}_n(-x_+)^n] = 0$. Our ω, on the other hand, can take any real value, and we allow for superpositions of in and out modes.

Chapter 7

Numerical results

Using the previously outlined methods, the response rate of the static detector for various values of the relevant parameters was numerically calculated. As mentioned earlier, the appropriate expression is (6.15). First, plotted in Fig. 7.1 is the transition rate for $r_+ = 0.1$, $r = 1$, summing from $l = 0$ to 4. The horizontal axis indicates the relative detector energy gap E/T_{loc} and the vertical axis indicates $L\dot{F}(E)$. While there are a number of different scales in this problem, assuming units such that $L = 1$ is the simplest way to make the transition rate dimensionless, so L is omitted in the axis labels following. The blue curve marked with circles indicates the Hartle-Hawking vacuum response, while the red curve with squares indicates the Boulware vacuum response. *Note that for this and the following graphs, the markers are intended as an aid to identifying the curves; the actual density of data points is much higher.* Convergence of the l sum can be easily verified by carrying out the summation to higher l order and comparing.

There are a couple notable features in the transition rate. First, note that for very large negative energy gap, corresponding to an initially excited detector, the Boulware and Hartle-Hawking vacuum responses are almost identical. Secondly, a number of spikes are observed, both in the Boulware and Hartle-Hawking vacuum response; in fact, the responses of both vacua are quite similar in the region of the plot where spikes occur. There do not appear to be any other interesting features in the regime where the different vacua produce different results: therefore we will henceforth focus on the Hartle-Hawking response.

Next, there are also a number of 'dips' in the response. This has a simple explanation: since the modes are real, there must be some energy for which a

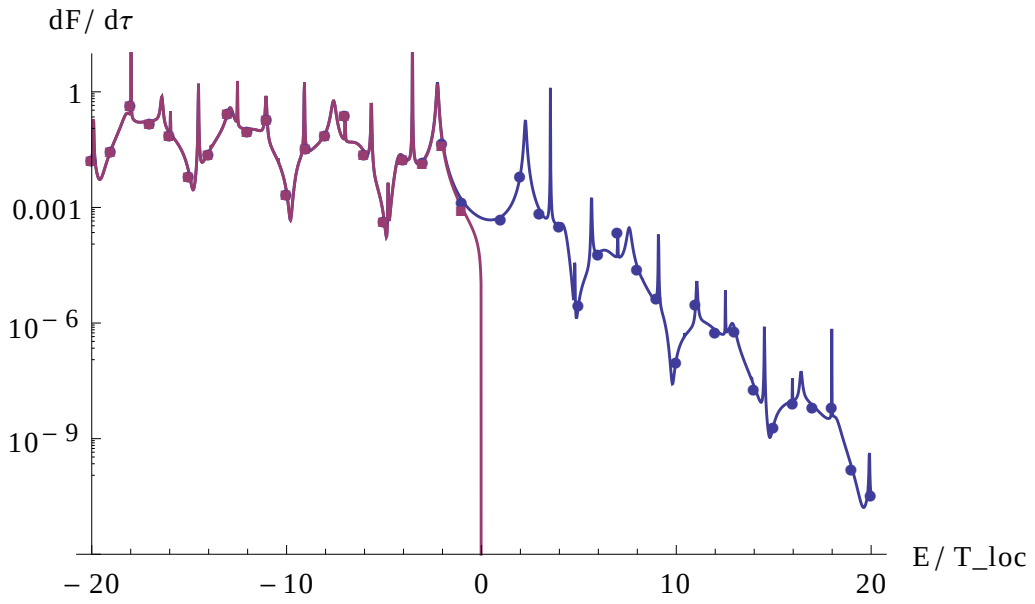

Figure 7.1: (Color online) The total static transition rate for $r_+ = 0.1, r = 1$. Hartle-Hawking vacuum in blue circles, Boulware in red squares. Note Boulware transition is zero for positive E. Markers not representative of data point density.

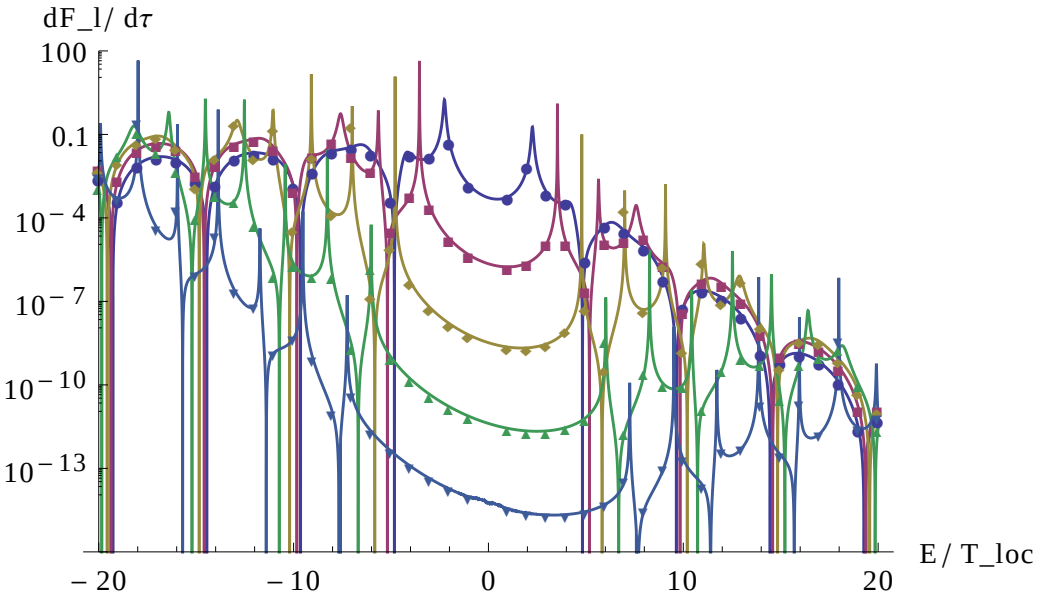

Figure 7.2: (Color online) Static transition rate contributions for $r_+ = 0.1, r = 1, l = 0, 1, .., 4$ from top to bottom.

zero of a mode crosses the location of the detector. Therefore, if one plotted the contributions of different l individually, one would see the transition rate go to zero. Indeed, this is visible in Fig. 7.2, where $l = 0$ is the top blue line with circles, $l = 1$ is the next line down in red with squares, and so on to $l = 4$.

Recall that the transition rate for detector gap E only depends on the modes at a particular energy $\tilde{\omega} = (E/T_{loc})T_H$. Therefore, the best way to compare transition rates at two different radii is to plot both of them against E/T_{loc} as we have done in Fig. 7.3, for $l = 2$; $r = 1$ is in blue circles, $r = 1.5$ in red squares. Notice how the peaks occur at the same locations, even as the zeroes shift. This suggests that our explanation for the zeroes is correct; the peaks will be addressed later.

Next, we plot the contributions of $l = 0, 1, 2, ..., 10$ for $r_+ = 1$, $r = 10$ in Fig. 7.4. Note that $r/r_+ = 10$ is kept constant; using this scaling allows us to compare situations with different black hole sizes, without worrying about scaling the detector into the horizon. In Fig. 7.4 once again $l = 0$ is the top line, $l = 1$ is the next line down, and so on.

Notice that the larger black hole appears to allow contributions from

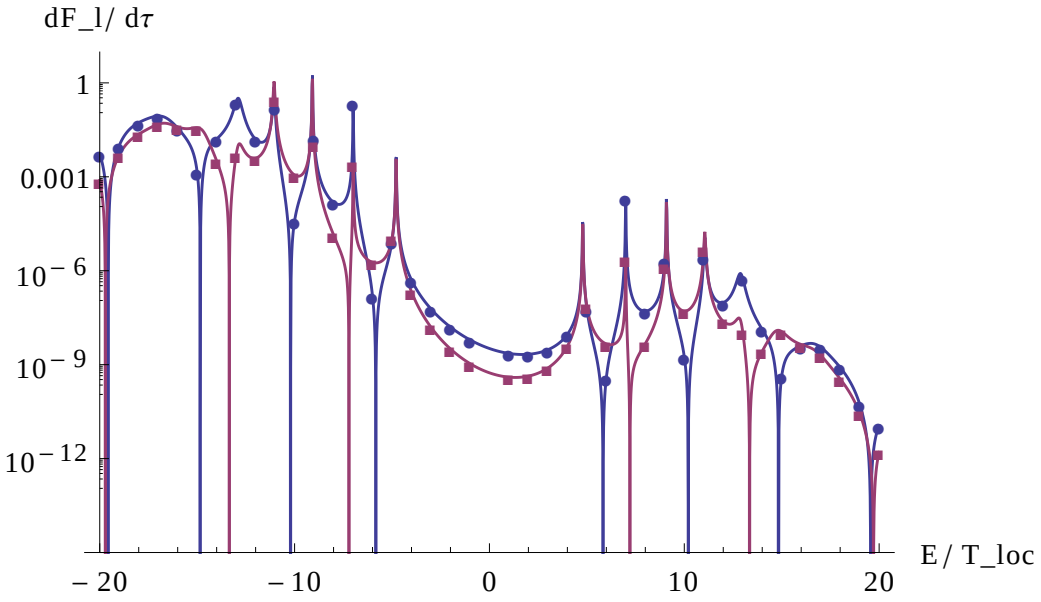

Figure 7.3: (Color online). Transition rate for different r. The static transition rate contribution for $r_+ = 0.1, l = 2, r = 1$ in blue circles, $r = 1.5$ in red squares.

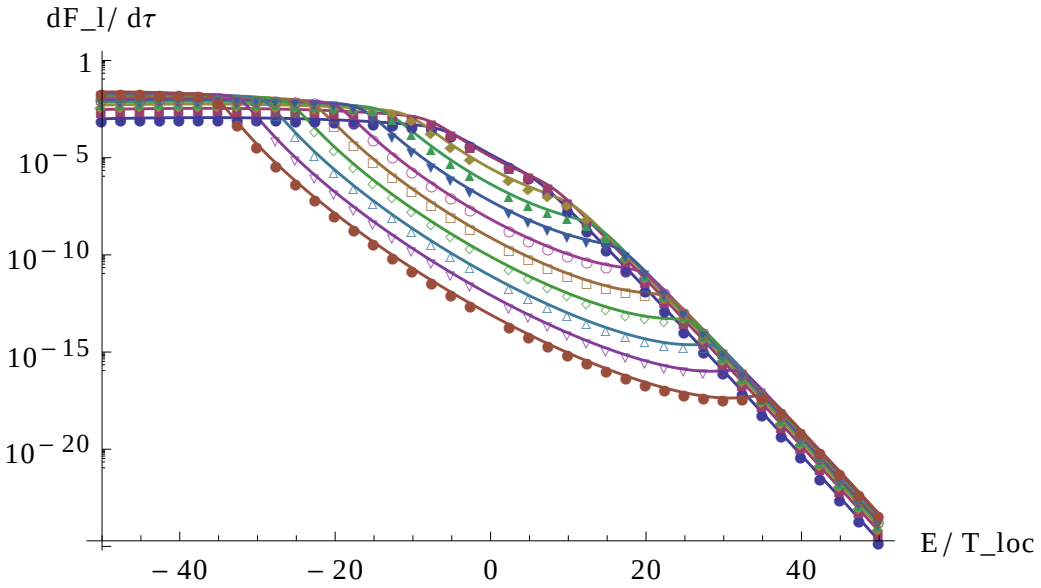

Figure 7.4: (Color online): Static transition rate contributions for $r_+ = 1$, $r = 10$, $l = 0, 1, ..., 10$ from top to bottom.

higher l modes. This makes sense, since we noted that near the horizon (and thus near the peak of the effective potential), the dependence of the potential on l decreases as r_+ increases. At low energies, as one would expect, the contribution from $l = 0$ is largest, followed by $l = 1$, and so forth. However, at higher energies, it appears as though the contributions for various l are comparable, up to some maximum. Of course, this means that if one wishes to calculate the total transition rate for $E/T_{loc} > 30$, one will need to consider higher l modes. This phenomenon is also visible in Fig. 7.2, but to a lesser extent; while the presence of the peaks confuses things somewhat, the $l = 2$ contribution does start being smaller than the $l = 0$ contribution at low energy, becoming comparable at larger energy.

The next graph, Fig. 7.5, shows the contributions of $l = 0, 1, 2$ for $r_+ = 0.01$, $r = 0.1$, with $l = 0$ at the top in blue circles, $l = 1$ below in red squares, and $l = 2$ at the bottom in yellow diamonds. Firstly, the suppression of higher l modes at smaller r_+ is clearly visible. Secondly, the 'spikiness' of the graph appears to have increased from the $r_+ = 0.1$ case—not only are the peaks at low energy sharper, but the peaks appear to be present at higher energies than in the $r_+ = 0.1$ case.

However, the graph is in some ways misleading. The higher l modes are much, much spikier than the lower l modes: the barely visible spike at $l = 2$, $E/T_{loc} \sim 1/2$ actually goes up to almost 10^9, although one requires more than ten digits of precision in E/T_{loc} to find the maximum of the peak properly. Unfortunately using this level of precision for the graph is not feasible, so the maximum heights of the peaks shown in the graphs are not completely accurate. The situation is comparable to that of Fig. 7.2, in which higher l modes can dominate at the peaks, but the peaks themselves are far thinner here.

In Fig. 7.5 our choice of scale for the horizontal axis appears to have placed the peaks in approximately the same places as in the $r_+ = 0.1$ case, Fig. 7.2; on the other hand, the exponential decrease of the transition rate with respect to increasing E appears to be more gradual. In other words, the relationship between the scale of the exponential decrease and the scale of the peaks changes as we manipulate the ratio of the black hole size to the AdS length (r_+/L). Going in the opposite direction, for $r_+ = 1$, naïvely applying scaling suggests that a peak should appear at about $E/T_{loc} = 20$; no peak is present, suggesting that the exponential decrease has overwhelmed the peaks entirely.

The observations in the previous paragraphs can be summarized as follows: In general, it appears that as $|E|$ is increased, the spikes visibly become shorter and broader, to the point where the peaks are not apparent at all; when r_+ is decreased, and as l increases, the spikes become taller and thinner, and persist at higher $|E|$. This is probably due to a competition between the exponential trend of the transition rate and the sharpness of the peaks: if r_+ is large enough, the exponential trend dominates, and the peaks cannot be seen. The *location* of the peaks appears to be on a different energy scale from the exponential decay; the relationship between these two scales changes as we change r_+/L.

The previous observations also seem to suggest a necessary precaution: when r_+/L is very small, the peaks at high l become quite extreme. Therefore, in order to properly represent the sum over all l at some energy, it appears that one must sum over all l which have peaks at lower energies, since we saw earlier that under certain circumstances, high l mode peaks can dominate over lower l modes.

We also briefly discuss the circular geodesic case. The transition rate is illustrated in Fig. 7.6 for $r_+ = 0.1$, $r = 1$, summing to $l = 4$, with the Boulware vacuum in red, and the Hartle-Hawking vacuum in blue. Once

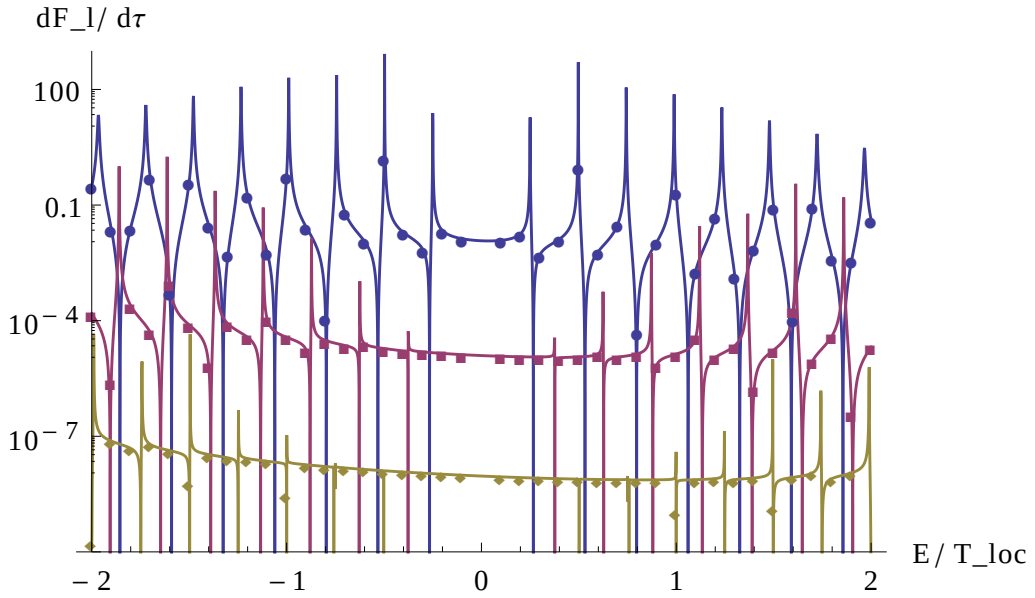

Figure 7.5: (Color online) The static transition rate contributions for $r_+ = 0.01, r = 0.1, l = 0, 1, 2$ from top to bottom.

again, for almost all $E < 0$, the two are almost exactly the same. Unlike the static case, however, the Boulware transition is nonzero for some $E > 0$. We will discuss it more later.

One notable feature is that the Hartle-Hawking transition appears "shifted" rightwards compared to the static graphs; it is no longer symmetric about $E = 0$, but instead about some positive energy. This is expected, since the detector is accelerating relative to static observers. Plotting the component l individually in Fig. 7.7 helps clarify what is going on here; once again, we have $l = 0$ in blue circles on the top, $l = 1$ in red squares below, and so on to $l = 4$.

At this point, it is apparent that each l appears more shifted than the last; the "centre" of each curve lies slightly farther to the right as l increases. The shift is such that each l dominates for a particular range of energies. The explanation lies in the definition of $\omega_- = (mb - E)/a$: for any positive E there will be some m such that ω_- takes its smallest positive value, and thus dominates; but $l \geq |m|$, and so this particular m can only be achieved for sufficiently large l. This is also why the Boulware transition rate appears to go to zero at some finite E—if one continued summation to higher l, one

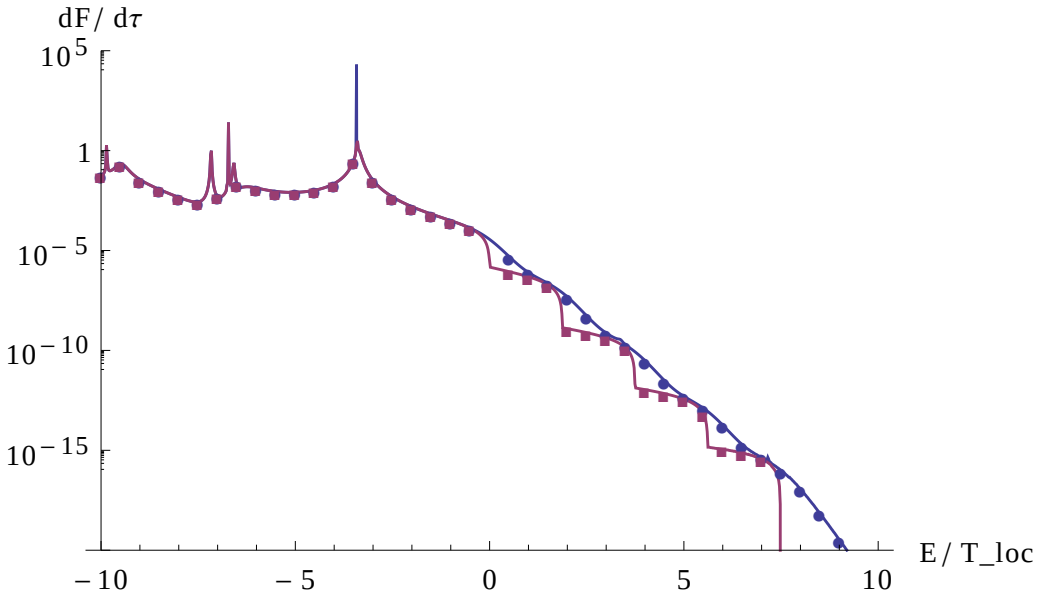

Figure 7.6: (Color online) Total circular geodesic transition rate contributions for $r_+ = 0.1, r = 1$. Hartle-Hawking vacuum in blue circles, Boulware vacuum in red squares

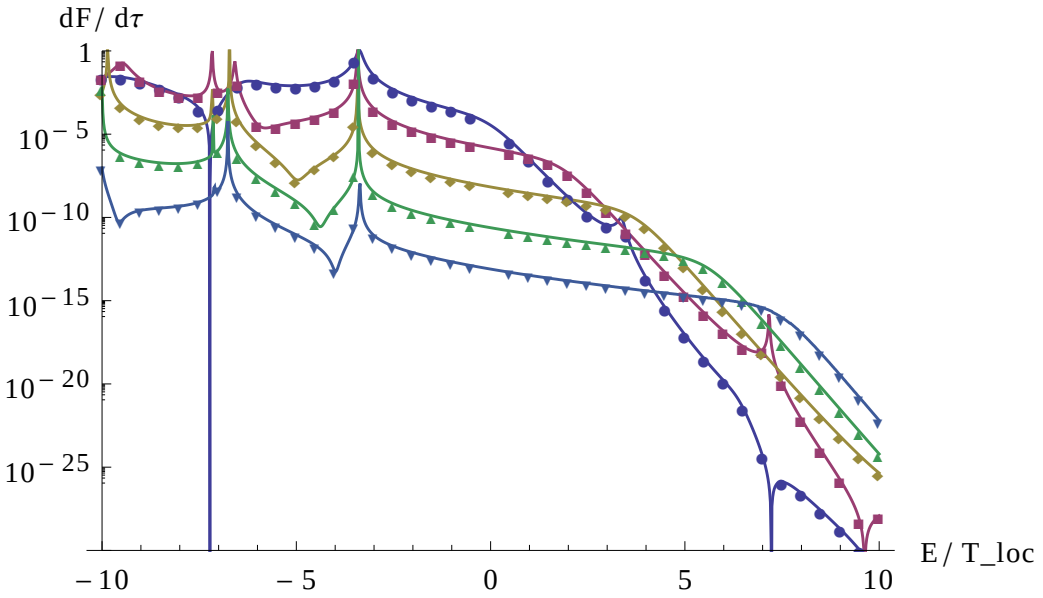

Figure 7.7: (Color online) Hartle-Hawking circular geodesic transition rate contributions for $r_+ = 0.1, r = 1, l = 0, 1, .., 4$ from top to bottom.

would see the transition rate stay nonzero at higher E. However, since the ω_- term occurs in both the Boulware and Hartle-Hawking responses, the nonzero transition rate at positive E should not be interpreted as a feature of the Hawking radiation; rather, it is a result of the circular *motion*.

It is also now clear why no peaks were visible for $E > 0$. While a small peak is visible in the $l = 0$ transition rate, for instance, the strong exponential decay suppresses it. In fact, the suppression is strong enough that the peak is 'hidden' by the higher l modes; at the energy where the $l = 0$ peak is located, both the $l = 1$ and $l = 2$ contributions are greater in magnitude, and their exponential trend masks the peak further.

For comparison, we include Fig. 7.8 for the Boulware transition rate. Note that the 'step' in the transition rate at zero seen in Fig. 7.6 is due solely to the $l = 0$ contribution; the higher l modes only vanish at higher energy. Specifically, each l contribution vanishes for $E = lb$, since this is the energy such that the highest ω_- becomes zero. This also explains the "steps" visible in the positive energy transition rate; each step simply corresponds to an l.

Besides that, however, the graphs appear to show precisely the same

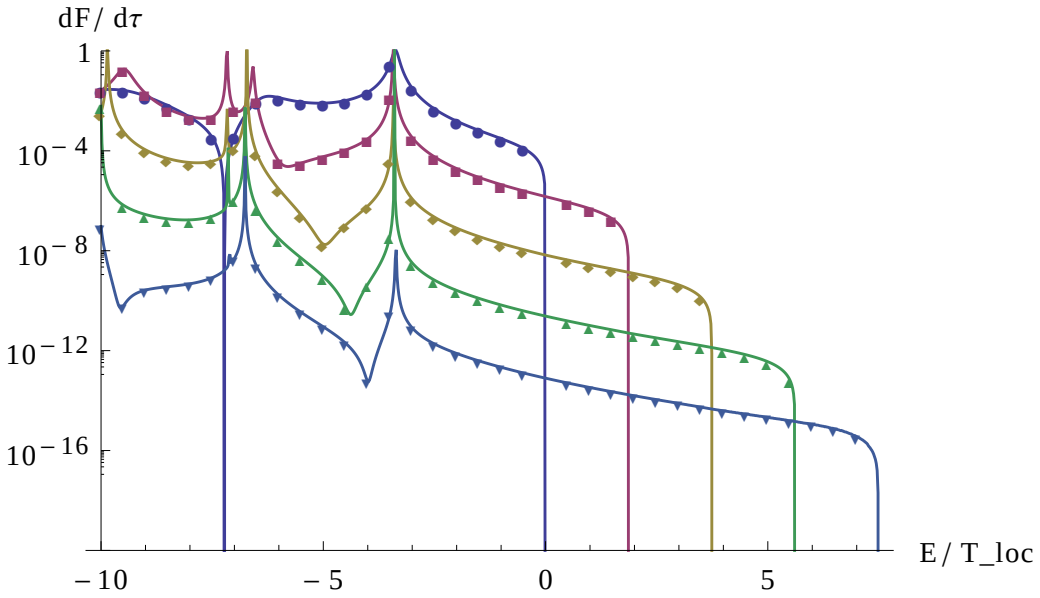

Figure 7.8: (Color online) Boulware circular geodesic transition rate contributions for $r_+ = 0.1, r = 1, l = 0, 1, .., 4$ from top to bottom.

features as observed in the static detector scenario, e.g. the characteristic peaks. Therefore, we will focus our analysis on the previous case.

Chapter 8

Analysis

We now discuss the peaks present in the static detector transition rate. At an abstract level, the spikes are reflective of resonances of the Klein-Gordon field over this spacetime—in other words, spikes occur when the frequency approaches a quasinormal frequency. While the literature on the analysis of quasinormal modes (QNMs) of black holes is rich (see Berti et al. [2009] for a recent review), the particular case of conformally coupled scalar fields on SAdS has not been fully explored at the present time—specifically, a table of quasinormal frequencies has not yet been calculated for this particular case. Therefore, we will use an alternate analysis.

Since the Klein-Gordon equations are equivalent to a scattering problem in one dimension, in tortoise coordinates, it makes sense to consider what happens if we have an incident wave from infinity with coefficient 1—that is, consider the following (approximate) solution to (6.6):

$$\tilde{R}^{scatter}_{\omega l} = \begin{cases} \frac{1}{\sqrt{\omega'}} \left(e^{-i\omega' r^*} + A e^{i\omega' r^*} \right) & r \to \infty \\ \frac{1}{\sqrt{\omega}} B e^{-i\omega r^*} & r \to r_+ \end{cases} \tag{8.1}$$

where $\omega'^2 = \omega^2 - l(l+1)$ is the squared wavenumber "at infinity", since $\tilde{V}$ does not vanish at infinity. We assume ω'^2 is positive, i.e. $\omega^2 > l(l+1)$. (While the regime $\omega^2 < l(l+1)$ may *a priori* bear some interesting phenomena, empirically this does not appear to be the case: there is no particular structure at energies below that of the first peak.) This solution to the Klein-Gordon equation is simply the incoming mode $\tilde{R}^{in}_{\omega l}$ from before, up to a constant coefficient.

There is a subtlety, however: since r^* is finite when r is infinite, the approximation requires that ω' is sufficiently large that the potential does

not change much over a wavelength. Again, in practice this assumption generally appears to be justified. More precisely, we use a Wentzel-Kramers-Brillouin (WKB) approximation; for wavenumber $k(r^*) = \sqrt{\omega^2 - \tilde{V}(r)}$, the validity condition is that $|k'(r^*)|/k^2(r^*) \ll 1/2\pi$, which holds for small black holes and far from the black hole. For instance, as $r^* \to 0$, $|k'(r^*)|/k^2(r^*) \to r_0/2\omega'^3$.

Then, since $\psi(r_+) = 1$, we must have

$$\tilde{R}^{in}_{\omega l} = \frac{\sqrt{\omega}}{B} \tilde{R}^{scatter}_{\omega l}, \tag{8.2}$$

which in turn implies that

$$\tilde{R}^{in}_{\omega l} = \begin{cases} \sqrt{\frac{\omega}{\omega'}} \frac{1}{B} \left(e^{-i\omega' r^*} + A e^{i\omega' r^*} \right) & r \to \infty \\ e^{-i\omega r^*} & r \to r_+ \end{cases} \tag{8.3}$$

Now, recall how we used this to get a mode satisfying the boundary condition: we set $\tilde{R}_{\omega l} = 2\,\mathrm{Im}[e^{-i\theta_0} \tilde{R}^{in}_{\omega l}]$. In this case, we can see that $\theta_0 = \mathrm{Arg}[\frac{A+1}{B}]$. So,

$$\tilde{R}_{\omega l} = \begin{cases} \sqrt{\frac{\omega}{\omega'}} \frac{2}{|B|} \,\mathrm{Im} \left(\frac{|A+1|}{A+1} \left(e^{-i\omega' r^*} + A e^{i\omega' r^*} \right) \right) & r \to \infty \\ 2\,\mathrm{Im}[e^{-i(\omega r^* + \theta_0)}] & r \to r_+ \end{cases} \tag{8.4}$$

We can clarify the situation by rewriting in terms of trigonometric functions. Specifically, near infinity, the physical modes must look like

$$\begin{aligned} \tilde{R}_{\omega l} &\to \sqrt{\frac{\omega}{\omega'}} \frac{2}{|B|} \,\mathrm{Im} \left(\frac{|A+1|}{A+1} \left(\frac{A+1}{2} \cos(\omega' r^*) \right. \right. \\ &\quad \left. \left. + i \frac{A-1}{2} \sin(\omega' r^*) \right) \right) \\ &= \sqrt{\frac{\omega}{\omega'}} \frac{|A+1|}{|B|} \,\mathrm{Im} \left(\cos(\omega' r^*) + i \frac{A-1}{A+1} \sin(\omega' r^*) \right) \\ &= \sqrt{\frac{\omega}{\omega'}} \frac{|A+1|}{|B|} \mathrm{Re} \left(\frac{A-1}{A+1} \sin(\omega' r^*) \right) \end{aligned} \tag{8.5}$$

The meaning of the last line is clarified if we use the identity $\frac{|A+1|}{A+1} = \frac{(A+1)^*}{|A+1|}$,

which results in

$$\begin{aligned}\tilde{R}_{\omega l} &\to \sqrt{\frac{\omega}{\omega'}}\frac{1}{|B||A+1|}\mathrm{Re}\left((A-1)(A+1)^*\sin(\omega' r^*)\right)\\ &= \sqrt{\frac{\omega}{\omega'}}\frac{1}{|B||A+1|}\mathrm{Re}\left((AA^*+A-A^*-1)\sin(\omega' r^*)\right)\\ &= \sqrt{\frac{\omega}{\omega'}}\frac{|A|^2-1}{|B||A+1|}\sin(\omega' r^*)\\ &= -\sqrt{\frac{\omega}{\omega'}}\frac{|B|}{|A+1|}\sin(\omega' r^*) \qquad (8.6)\end{aligned}$$

where the last equation follows from the fact that $|A|^2 + |B|^2 = 1$ in our approximation. (Of course, near the horizon, $\tilde{R}_{\omega l} \to -2\sin(\omega r^* + \theta_0)$, which we previously demanded in order to satisfy normalization.)

An explanation for the peaks now presents itself: one must experience a peak when the reflection coefficient A approaches -1, i.e. the phase of A approaches π. This corresponds to having $\tilde{R}^{in}_{\omega l}(r \to \infty)$ approach 0 — in other words, it is much like having the incoming (at the horizon) mode satisfy the boundary condition at infinity. Of course, those boundary conditions are precisely those satisfied by the quasinormal modes, so we have come full circle.

The previous derivation has a small caveat: we relied on the WKB approximation to determine the behaviour of the mode near infinity. However, the validity condition typically is not satisfied at the particular r of the detector and the energies of the peaks shown in the graphs. One can relax the validity condition by allowing the amplitude to change with r^*, which corresponds to taking a higher order WKB approximation; in that case, one would see that the amplitude smoothly interpolates from 2 near the horizon to a large value at infinity, so a large amplitude at infinity indicates a large amplitude at any intermediate distance, and thus a peak in the detector transition rate.

Besides avoiding the invocation of QNMs, the analysis above additionally allows us to make qualitative predictions regarding the peaks. For instance, assuming the phase of A changes much faster than its magnitude (which appears to be the case when r_+ is sufficiently small), the local maxima of the coefficient $C = |B|/|A+1|$ in (8.6) occur when A is negative real, and are

$$C = \frac{|B|}{1-|A|} = \frac{\sqrt{1-|A|^2}}{1-|A|},$$

while the local minima occur when A is positive real, and are

$$C = \frac{|B|}{1+|A|} = \frac{\sqrt{1-|A|^2}}{1+|A|}.$$

The maxima and minima are both 1 when $|A| = 0$; as $|A| \to 1$, the maxima monotonically increase towards infinity, while the minima monotonically approach zero. Since one expects $|A| \to 0$ as $\omega^2 \to \infty$, peakiness decreases as energy increases; conversely, as energy decreases, peakiness must increase. Of course, there is a peak of lowest energy, i.e. a lowest energy QNM, so there will not be an infinite sequence of higher and higher peaks as $\omega^2 \to 0$. Additionally, the fact that l corresponds to a higher effective potential suggests that as l increases, the real part of the frequency of the lowest-lying QNM will also increase—in other words, it suggests that the peaks will occur at higher energies. The exact relationship between A and ω, however, must be calculated.

As an aside, if we translate the above predictions into the language of QNMs, we are essentially predicting that as the real part of the QNM increases in magnitude, the imaginary part also increases in magnitude; and that as l increases, so does the real part of the QNM. This agrees with the behaviour of QNMs in SAdS for other couplings (e.g. minimal) noted in the literature (see Berti et al. [2009] for a thorough survey).

We may also compare the peaks found here to the more familiar case of normal modes in AdS. Following the approach found in Burgess and Lütken [1985], using effective mass $\mu^2 = -2R^2$ to yield a conformal coupling, we find that the normal mode frequencies corresponding to our coupling and boundary conditions are

$$\omega L = 2 + l + 2n. \tag{8.7}$$

Notably, this is quite similar to the frequencies of the minimally coupled modes, $\omega L = 3 + l + 2n$.

In order to translate the peak detector energies E into mode energies, recall that $\tilde{\omega} = \sqrt{f(r)}E$; therefore,

$$E/T_{loc} = \tilde{\omega}/T_H \tag{8.8}$$

Using this equation, we can observe from the graphs that the peaks converge to the AdS normal conformal modes as $r_+ \to 0$: for instance, when $r_+ = 0.01$, $T_H = 7.96$, so the first peak $(l = 0, n = 0)$ corresponds to a mode frequency

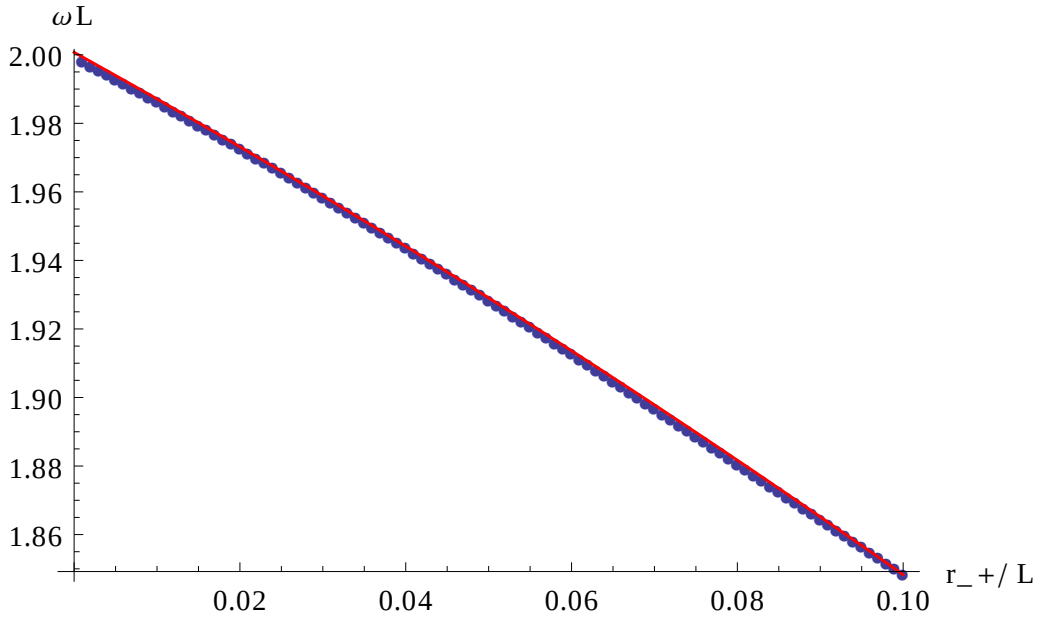

Figure 8.1: (Color online) Frequency corresponding to the peak of the static transition rate with respect to black hole size, for small black holes (thick dotted line). A quadratic fit (red solid line) has been overlaid on the peak frequencies.

of about 2.0. This makes sense—the smaller the black hole is, the smaller its "influence" over the volume of AdS.

In order to verify the convergence to the AdS normal mode limit, we plotted the location (i.e. the corresponding mode frequency) of the first peak in the $l = 0$ transition rate, corresponding to $n = 0$, with respect to the black hole size. The results are plotted in Fig. 8.1: similarly to the minimally coupled case mentioned in Berti et al. [2009], the trend is linear as $r_+ \to 0$, with a very slight next-order (i.e. quadratic) term visible; a quadratic fit has been plotted on the graph. This strongly suggests that the frequency of the SAdS QNMs is tied to the AdS scale, rather than the Schwarzschild scale, at least for small black holes.

There is a sense in which this limit is counter-intuitive, however. If we consider a black hole of constant radius and alter the cosmological constant, one might expect that as the cosmological constant approaches zero, the response function should approximate that of the Schwarzschild spacetime.

At first, this appears to be contradicted by the increasing 'peakiness' of the calculated response. However, there is a sense in which such a limit may exist: if we consider the transition rate at a constant energy with respect to the local temperature (in contrast to the scales chosen above, which corresponded to the AdS scale), and change the cosmological constant, the peaks will come closer and closer together. It is possible that in the small Λ limit, the peaks become indistinguishable, and the transition rate appears smooth. This is quite reminiscent of how, as the number of quanta is increased, a quantum system can approach a classical limit, e.g. the Rydberg atom.

While this interpretation seems plausible, it is not trivial to verify it. Confirming the existence of this limit would require analysis of the asymptotics of the transition rate: specifically, one would have to determine the height and location of each peak, then determine the 'average' contribution of each order of l. This would likely require characterization of the Wightman function in terms of a sum over poles in the complex frequency plane (i.e. quasinormal frequencies). Since the quasinormal frequencies in the conformal coupling case have not been fully characterized, we do not attempt this analysis at this time.

The analogue of the limit $r_+ \to \infty$ is rather less clear. First, while not shown in the graph in Fig. 8.1, when r_+ is sufficiently large, the peak disappears; it is simply suppressed by the larger-scale trend of exponential decay in the transition rate. Even before then, some behaviour is visible that departs from the quadratic fit done on the previous graph, as can be seen in Fig. 8.2; there is an increase in peak frequency over the general trend above the quadratic fit done in the previous case. As well, the peak in the transition rate disappears completely just beyond the end of the region plotted. It is likely that the reason for the deflection is that the peak is being "shifted" by the exponential term in the transition rate; in that case, the true location of the QNM no longer corresponds to the peak of the transition rate.

Physically, as r_+ is increased, the horizon moves 'towards' the SAdS conformal boundary; or, if one chooses to keep the horizon radius constant and scale the AdS radius instead, the cosmological constant becomes larger and larger in magnitude, and the conformal boundary moves towards the horizon. However, neither of these scalings appear to approach the intuitive limits. Since the lower-energy peaks disappear, the response function does not approach that of AdS. This limit is also quite unlike the Schwarzschild black hole in flat space; since the reflecting boundary is still present, the higher l modes will still suffer sharper peaks. It is not simply a matter

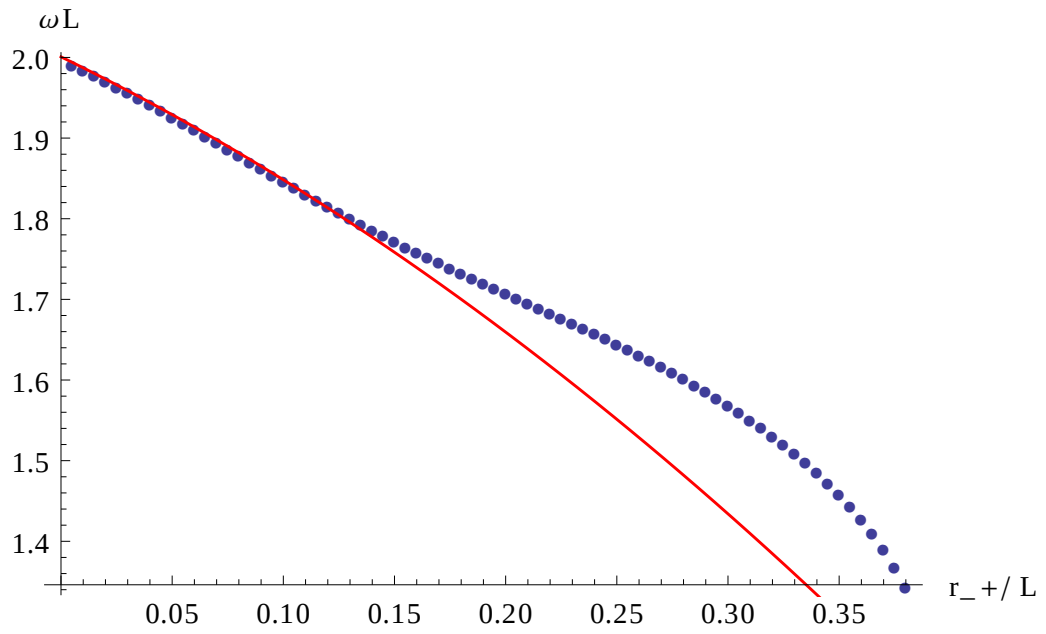

Figure 8.2: (Color online) Frequency corresponding to the peak of the static transition rate with respect to black hole size, for larger black holes (thick dotted line). The quadratic fit displayed in Fig. 8.1 (red solid line) is also plotted here.

of placing a reflecting sphere very near the Schwarzschild black hole in flat space, either—since the effective potential always has a peak within SAdS, any reflecting sphere would have to stay outside the peak of the effective potential in the Schwarzschild-flat case. In fact, this limit is *also* unlike the minimally coupled case: in that case, a sufficiently large SAdS black hole has no local maximum in the effective potential outside the horizon (see e.g. Berti et al. [2009]), while our conformally coupled case always does. In the end, it is probably better to consider the limit of a large black hole as a different physical situation entirely; the QNMs in that case may not converge to any more familiar form, and in any case may not be of any relevance to the transition rate.

Chapter 9

Conclusion and outlook

We have computed, for the four-dimensional Schwarzschild anti-de Sitter spacetime, the response of an Unruh-DeWitt detector in static and circular geodesic trajectories to a conformally coupled scalar field. The response function bears some sharp peaks with respect to the detector energy gap; we have demonstrated that these spikes are due to quasinormal mode resonances. There are also some troughs in the graph; when the contributions are separated by l, it becomes clear that this corresponds to when a zero of the mode function crosses the location of the detector.

We have also attempted to characterize the dependence of the location of the peaks on the radius of the black hole in AdS space. Qualitatively, the spikes are only visible when the black hole is much smaller than the AdS length; as the black hole's size is decreased, the spikes appear sharper and higher. One might have expected a transition between small, intermediate, and large black holes, in analogy with the minimally coupled case. However, this type of transition cannot occur in this case: the effective potential of the conformally coupled scalar field always has a maximum at finite distance, and as a result, no phenomena related to the phase transition are apparent in the conformally coupled scalar field. Our computation of the peak frequencies at various black hole sizes confirms the convergence of the peak frequency as $r_+ \to 0$ to the AdS normal frequencies; the disappearance of peaks at higher black hole size appears to be mainly due to the dominance of the exponential decay term over the peak, rather than any sort of phase transition of the spacetime as a whole.

We would like to note that the calculation of the static and circular geodesic transition rates is a first step towards characterizing the response of

the detector to Hawking radiation on more general trajectories, e.g. radial geodesic infall. Remarkably, the Unruh-DeWitt detector formalism used here can also be applied to even more general physical scenarios, such as calculating the evolution of the entanglement of two detectors above the black hole, a calculation that would be relevant for the study of the dynamics of correlations and information near black hole horizons. That, in turn, would shed some light both on the question of information loss, which has been carefully investigate for much time, and on the question of black hole firewalls, a relatively new dilemma which has invited further study.

Looking further ahead, the unification of quantum physics and general relativity is one of the central goals of physics in the twenty-first century; physicists hope to discover a theory that describes everything, from the smallest particles to the largest structures in the universe. Black holes and AdS space offer glimpses of how such a theory might work; understanding them is key to understanding our universe. Our work in analyzing the response of an Unruh-DeWitt detector to AdS black hole radiation is a small step towards that formidable goal.

Bibliography

Álvaro M. Alhambra, Achim Kempf, and Eduardo Martín-Martínez. Casimir forces on atoms in optical cavities. *Phys. Rev. A*, 89: 033835, Mar 2014. doi: 10.1103/PhysRevA.89.033835. URL `http://link.aps.org/doi/10.1103/PhysRevA.89.033835`.

Ahmed Almheiri, Donald Marolf, Joseph Polchinski, and James Sully. Black Holes: Complementarity or Firewalls? *JHEP*, 1302:062, 2013. doi: 10.1007/JHEP02(2013)062.

S.J. Avis, C.J. Isham, and D. Storey. Quantum field theory in anti-de sitter space-time. *Phys. Rev. D*, 18:3565–3576, Nov 1978. doi: 10.1103/PhysRevD.18.3565. URL `http://link.aps.org/doi/10.1103/PhysRevD.18.3565`.

Zvi Bern, Lance J. Dixon, and Radu Roiban. Is N = 8 supergravity ultraviolet finite? *Phys.Lett.*, B644:265–271, 2007. doi: 10.1016/j.physletb.2006.11.030.

Emanuele Berti, Vitor Cardoso, and Andrei O. Starinets. Quasinormal modes of black holes and black branes. *Class.Quant.Grav.*, 26:163001, 2009. doi: 10.1088/0264-9381/26/16/163001.

N.D. Birrell and P.C.W. Davies. *Quantum Fields in Curved Space*. Cambridge Monographs on Mathematical Physics. Cambridge University Press, 1984. ISBN 9780521278584.

Eric G. Brown, Eduardo Martín-Martínez, Nicolas C. Menicucci, and Robert B. Mann. Detectors for probing relativistic quantum physics beyond perturbation theory. *Phys. Rev. D*, 87: 084062, Apr 2013. doi: 10.1103/PhysRevD.87.084062. URL `http://link.aps.org/doi/10.1103/PhysRevD.87.084062`.

C.P. Burgess and C.A. Lütken. Propagators and effective potentials in anti-de sitter space. *Physics Letters B*, 153(3):137 – 141, 1985. ISSN 0370-2693. doi: http://dx.doi.org/10.1016/0370-2693(85)91415-7. URL http://www.sciencedirect.com/science/article/pii/0370269385914157.

J.S.F. Chan and Robert B. Mann. Scalar wave falloff in asymptotically anti-de Sitter backgrounds. *Phys.Rev.*, D55:7546–7562, 1997. doi: 10.1103/PhysRevD.55.7546.

S. M. Christensen and S. A. Fulling. Trace anomalies and the hawking effect. *Phys. Rev. D*, 15:2088–2104, Apr 1977. doi: 10.1103/PhysRevD.15.2088. URL http://link.aps.org/doi/10.1103/PhysRevD.15.2088.

Ramin G. Daghigh and Michael D. Green. Highly Real, Highly Damped, and Other Asymptotic Quasinormal Modes of Schwarzschild-Anti De Sitter Black Holes. *Class.Quant.Grav.*, 26:125017, 2009. doi: 10.1088/0264-9381/26/12/125017.

B. DeWitt. *General Relativity; an Einstein Centenary Survey*. Cambridge University Press, Cambridge, UK, 1980.

Alessandro Fabbri and Jose Navarro-Salas. *Modeling black hole evaporation*. World Scientific, London (United Kingdom), June 2005.

V. Frolov and I.D. Novikov. *Black Hole Physics: Basic Concepts and New Developments*. Fundamental Theories of Physics. Springer Netherlands, 1998. ISBN 9780792351450. URL http://books.google.ca/books?id=n0kHI6CVWZUC.

S.A. Fulling. *Aspects of Quantum Field Theory in Curved Spacetime*. London Mathematical Society Student Texts. Cambridge University Press, 1989. ISBN 9780521377683. URL http://books.google.ca/books?id=Zo5_3cmtFEUC.

Stephen A. Fulling. Nonuniqueness of canonical field quantization in riemannian space-time. *Phys. Rev. D*, 7:2850–2862, May 1973. doi: 10.1103/PhysRevD.7.2850. URL http://link.aps.org/doi/10.1103/PhysRevD.7.2850.

J.B. Hartle and S.W. Hawking. Path-integral derivation of black-hole radiance. *Phys. Rev. D*, 13:2188–2203, Apr 1976. doi: 10.1103/PhysRevD.13.2188. URL `http://link.aps.org/doi/10.1103/PhysRevD.13.2188`.

S.W. Hawking. Black hole explosions. *Nature*, 248:30–31, 1974. doi: 10.1038/248030a0.

S.W. Hawking. Particle creation by black holes. *Communications in Mathematical Physics*, 43(3):199–220, 1975. ISSN 0010-3616. doi: 10.1007/BF02345020. URL `http://dx.doi.org/10.1007/BF02345020`.

S.W. Hawking and Don N. Page. Thermodynamics of Black Holes in anti-De Sitter Space. *Commun.Math.Phys.*, 87:577, 1983. doi: 10.1007/BF01208266.

Samuli Hemming and Esko Keski-Vakkuri. Hawking radiation from AdS black holes. *Phys.Rev.*, D64:044006, 2001. doi: 10.1103/PhysRevD.64.044006.

Lee Hodgkinson. *Particle detectors in curved spacetime quantum field theory*. PhD thesis, School of Mathematical Sciences, University of Nottingham, Nottingham, NG7 2RD, UK, 2013.

Lee Hodgkinson, Jorma Louko, and Adrian C. Ottewill. Static detectors and circular-geodesic detectors on the schwarzschild black hole. *Phys. Rev. D*, 89:104002, May 2014. doi: 10.1103/PhysRevD.89.104002. URL `http://link.aps.org/doi/10.1103/PhysRevD.89.104002`.

Gary T. Horowitz and Veronika E. Hubeny. Quasinormal modes of AdS black holes and the approach to thermal equilibrium. *Phys.Rev.*, D62:024027, 2000. doi: 10.1103/PhysRevD.62.024027.

Veronika E. Hubeny, Donald Marolf, and Mukund Rangamani. Hawking radiation from AdS black holes. *Class.Quant.Grav.*, 27:095018, 2010. doi: 10.1088/0264-9381/27/9/095018.

Benito A. Juárez-Aubry and Jorma Louko. Onset and decay of the 1+1 Hawking-Unruh effect: what the derivative-coupling detector saw. 2014.

Jorma Louko and Alejandro Satz. Transition rate of the Unruh-DeWitt detector in curved spacetime. *Class.Quant.Grav.*, 25:055012, 2008. doi: 10.1088/0264-9381/25/5/055012.

Juan Martin Maldacena. The Large N limit of superconformal field theories and supergravity. *Adv.Theor.Math.Phys.*, 2:231–252, 1998.

Eduardo Martín-Martínez, Miguel Montero, and Marco del Rey. Wavepacket detection with the unruh-dewitt model. *Phys. Rev. D*, 87:064038, Mar 2013. doi: 10.1103/PhysRevD.87.064038. URL `http://link.aps.org/doi/10.1103/PhysRevD.87.064038`.

Marlan O. Scully and M. Suhail Zubairy. *Quantum Optics*. Cambridge University Press, 1997.

L. Smolin. The case for background independence. *ArXiv High Energy Physics - Theory e-prints*, July 2005.

W.G. Unruh. Notes on black-hole evaporation. *Phys. Rev. D*, 14:870–892, Aug 1976. doi: 10.1103/PhysRevD.14.870. URL `http://link.aps.org/doi/10.1103/PhysRevD.14.870`.

Edward Witten. Anti-de Sitter space and holography. *Adv.Theor.Math.Phys.*, 2:253–291, 1998.

Appendix A

Derivation of the Hartle-Hawking Wightman function

The Hartle-Hawking vacuum can be constructed by computing the Bogoliubov coefficients of the external modes with respect to the Kruskal modes [Hemming and Keski-Vakkuri, 2001]. While the Dirichlet boundary condition presents a slight complication, the derivation proceeds much like the Schwarzschild case.

In this particular case, we have what is essentially a reflecting boundary at infinity, and so we only have one basis of modes on each exterior, rather than Schwarzschild's two; the situation is analogous to that of the black hole in a reflecting boundary analyzed in Frolov and Novikov [1998]. Consider the mode given in (6.7):

$$\begin{aligned} w_{\omega lm} &= (4\pi\omega)^{-1/2} r^{-1} e^{-i\omega t} Y_{lm}(\theta,\phi) \\ &\quad (-i)\left(e^{-i\theta_0} e^{-i\omega r^*}\psi^{in}_{\omega l} - e^{i\theta_0} e^{i\omega r^*}\psi^{out}_{\omega l}\right). \end{aligned} \tag{A.1}$$

It fulfils the boundary condition at infinity, and is a positive frequency superposition of in and out modes. We can express it in terms of u, v as

$$\begin{aligned} w_{\omega lm} &= (4\pi\omega)^{-1/2} r^{-1} Y_{lm}(\theta,\phi) \\ &\quad (-i)\left(e^{-i\theta_0} e^{-i\omega v}\psi^{in}_{\omega l} - e^{i\theta_0} e^{-i\omega u}\psi^{out}_{\omega l}\right). \end{aligned} \tag{A.2}$$

Next, we consider the behaviour of these physical modes inside the black

hole. Rewriting in terms of U, V, we get

$$w_{\omega lm} = (4\pi\omega)^{-1/2} r^{-1} Y_{lm}(\theta, \phi)$$
$$(-i)\left(e^{-i\theta_0} V^{-\frac{i\omega}{2\pi T_H}} \psi^{in}_{\omega l} - e^{i\theta_0}(-U)^{\frac{i\omega}{2\pi T_H}} \psi^{out}_{\omega l}\right). \tag{A.3}$$

We then analytically continue to the parallel exterior of the black hole, crossing the singularities at $UV = 0$ by analytic continuation in the lower half-plane in both U and V. Note that the part involving ψ^{in} is regular across $U = 0$ and the part involving ψ^{out} is regular across $V = 0$. The rest of the derivation follows quite similarly to the Schwarzschild case [Christensen and Fulling, 1977]: we compute the Bogoliubov coefficients of the physical mode relative to the Kruskal modes and find

$$\langle\Psi|\, a^\dagger_{\omega lm} a_{\omega lm}\, |\Psi\rangle = \frac{1}{e^{\omega/T_H} - 1}, \tag{A.4}$$

$$\langle\Psi|\, a_{\omega lm} a^\dagger_{\omega lm}\, |\Psi\rangle = \frac{1}{1 - e^{-\omega/T_H}}, \tag{A.5}$$

where we write the annihilator of the usual physical mode as $a_{\omega lm}$, the state $|\Psi\rangle = |0_K\rangle$ is the Hartle-Hawking vacuum (i.e. the Kruskal vacuum), and all other operator combinations vanish. Note that this is a Bose-Einstein distribution, as expected [Fabbri and Navarro-Salas, 2005].

Using the field operator in (6.11) and these operator relations, we arrive at our final result,

$$\begin{aligned} W(x, x') &= \langle\Psi|\, \phi(x)\phi(x')\, |\Psi\rangle \\ &= \sum_{l=0}^{\infty} \sum_{m=-l}^{l} \int_0^\infty d\omega \\ &\left[\frac{w_{\omega lm}(x) w^*_{\omega lm}(x')}{1 - e^{-\omega/T_H}} + \frac{w^*_{\omega lm}(x) w_{\omega lm}(x')}{e^{\omega/T_H} - 1}\right] \\ &= \sum_{l=0}^{\infty} \sum_{m=-l}^{l} \int_0^\infty \frac{d\omega}{2\sinh(\omega/2T_H)} \\ &\left[e^{\omega/2T_H} w_{\omega lm}(x) w^*_{\omega lm}(x')\right. \\ &\left.+ e^{-\omega/2T_H} w^*_{\omega lm}(x) w_{\omega lm}(x')\right]. \end{aligned} \tag{A.6}$$